Doppler Noise Considered as a Function of the Signal Path Integration of Electron Density

A. L. Berman and J. A. Wackley
Network Operations Section

This article advances the hypothesis that observed doppler noise during solar conjunctions is proportional to total columnar electron content along the signal path. This assumption leads directly to a geometrical model ("ISED") for observed doppler noise which is shown to be in very good agreement with doppler noise data accumulated during the 1975 Pioneer 10, Pioneer 11 and Helios 1 solar conjunctions. An augmented model ("RISED") is constructed which quantitatively indicates correlation between Earth observed Sunspot activity and systematic, cyclical deviations from the ISED model. Applications expected from this effort are: (1) Ability to validate generation of doppler data during solar conjunctions, (2) Ability to predict solar corruption of doppler data during mission critical phases which occur during solar conjunctions, and (3) Possibility of extracting electron density information from observed doppler noise.

I. Introduction

In 1975, A. L. Berman and S. T. Rockwell, after studying the (1975) solar conjunctions of the Pioneer 10, Pioneer 11, and Helios 1 spacecraft, proposed (see Reference 1) a geometrical doppler noise model (NOISE_p) as follows:

$$\text{NOISE}_p(Hz) = \begin{cases} 0.003; & ISI \leq 223 \\ K_1(ISI)^{1+K_2}; & ISI > 223 \end{cases}$$

where

$$ISI = \frac{\beta}{\sin \alpha}$$

α = Sun-Earth-probe angle (SEP), deg

β = Earth-Sun-probe angle (ESP), deg

$K_1 = 2.8 \times 10^{-6}$

$K_2 = 2.9 \times 10^{-1}$

Basically, the NOISE$_p$ model was derived by noting that possible sources of solar corruption of doppler data, such as electromagnetic energy flux and charged particles, had densities roughly proportional to the inverse square of the distance from the Sun, and then hypothesizing that the total effect leading to an increase in doppler data noise would be obtained by integrating the density of corrupting sources along the signal path:

$$\text{doppler noise} = K\int \frac{1}{r^2}\,dR$$

where

r = Sun–signal path distance

R = Earth–spacecraft distance

K = arbitrary constant

with the result that

$$\int \frac{1}{r^2}\,dR = \frac{1}{r_e}\left(\frac{\beta}{\sin\alpha}\right)$$

A better fit to actual (observed) doppler noise data[1] was obtained by raising *ISI* to the 1.29 power, thus leading to the final model form (NOISE $_p$).

It was subsequently concluded that the derived parameter *ISI* was extremely similar to expressions given for total (solar) electron content along the signal path. For instance, L. Efron and R. J. Lisowski (Ref. 2) give the identical (functional) expression for total signal path electron content

$$I_e = \int N_e(r)\,dR = \frac{N_1}{r_e}\frac{\beta}{\sin\alpha}$$

where

I_e = total electron content along signal path

$N_e(r)$ = electron density function

N_1 = electron density at $r = r_e$

r_e = Earth-Sun distance (AU)

It was then considered that perhaps a better model could be obtained if one used a more precise expression (i.e., not simply $1/r^2$) for the electron density function. A great many expressions to define the solar electron density as a function of distance from the Sun have been advanced during the last several decades, and they are all somewhat similar. Typical examples are (with r = distance from the Sun):

Van De Hulst: $N_e(r) = \frac{A}{r^6} + \frac{B}{r^{2.3}}$ (Ref. 3)

Hollweg: $N_e(r) = \frac{A}{r^6} + \frac{B}{r^2}$ (Ref. 4)

Muhleman: $N_e(r) = \frac{A}{r^6} + \frac{B}{r^{2.3}}$ (Ref. 5)

The Muhleman formulation above was selected, and Section II proceeds to evaluate the following expression:

$$I_e = \int N_e(r)\,dR = \int\left(\frac{C_1}{r^6} + \frac{C_0}{r^{2.3}}\right)dR$$

II. Signal Path Integration of the Muhleman Electron Density Function: The "ISED" Model

One wishes to obtain I_e:

$$I_e = \int\left(\frac{C_1}{r^6} + \frac{C_0}{r^{2.3}}\right)dR = C_1\int\frac{dR}{r^6} + C_0\int\frac{dR}{r^{2.3}}$$

Figure 1 details the Earth-Sun-spacecraft geometry, with

$r^2 = R^2 + r_e^2 - 2Rr_e\cos\alpha$

$r_{s/c}$ = Earth-spacecraft distance

$R_{s/c}$ = spacecraft-Sun distance

Starting with the $C_0/r^{2.3}$ term, one has:

$$I_{e1} = C_0\int_0^{R_{s/c}}\frac{dR}{r^{2.3}} = C_0\int_0^{R_{s/c}}\frac{dR}{(R^2 + r_e^2 - 2Rr_e\cos\alpha)^{1.15}} = C_0\int_0^{R_{s/c}}\frac{dR}{([R - r_e\cos\alpha]^2 + r_e^2\sin^2\alpha)^{1.15}}$$

[1]All references to observed doppler noise will be taken to mean "pass average," good, two-way 60-second sample rate doppler data noise (see Refs. 1 and 7 for greater detail).

Let

$$x = R - r_e \cos\alpha$$

$$dx = dR$$

$$a = r_e \sin\alpha$$

so that

$$I_{e1} = C_0 \int_{-r_e\cos\alpha}^{R_{s/c} - r_e\cos\alpha} \frac{dx}{(x^2 + a^2)^{1.15}}$$

$$= \frac{C_0}{a^{2.3}} \int_{-r_e\cos\alpha}^{R_{s/c} - r_e\cos\alpha} \frac{dx}{\left(1 + \frac{x^2}{a^2}\right)^{1.15}}$$

Now let

$$\frac{x}{a} = \tan w$$

$$dx = a\sec^2 w dw$$

so that

$$I_{e1} = \frac{C_0}{a^{2.3}} \int_{\tan^{-1}\frac{(-r_e\cos\alpha)}{a}}^{\tan^{-1}\frac{(R_{s/c} - r_e\cos\alpha)}{a}} \frac{a\sec^2 w dw}{(\tan^2 w + 1)^{1.15}}$$

$$= \frac{C_0}{a^{1.3}} \int_{\tan^{-1}\frac{(-r_e\cos\alpha)}{a}}^{\tan^{-1}\frac{(R_{s/c} - r_e\cos\alpha)}{a}} \frac{dw}{(\tan^2 w + 1)^{0.15}}$$

and since

$$\tan^2 w + 1 = \sec^2 w = \frac{1}{\cos^2 w}$$

then

$$I_{e1} = \frac{C_0}{a^{1.3}} \int_{\tan^{-1}\frac{(-r_e\cos\alpha)}{a}}^{\tan^{-1}\frac{(R_{s/c} - r_e\cos\alpha)}{a}} (\cos w)^{0.3} dw$$

From Ref. 1, p. 237:

$$\tan^{-1}\left(-\frac{r_e\cos\alpha}{a}\right) = \alpha - \frac{\pi}{2}$$

and

$$\frac{R_{s/c} - r_e\cos\alpha}{r_e\sin\alpha} = \tan\left(\beta - \left[\frac{\pi}{2} - \alpha\right]\right)$$

$$\tan^{-1}\left(\frac{R_{s/c} - r_e\cos\alpha}{a}\right) = \beta - \left[\frac{\pi}{2} - \alpha\right]$$

$$= \beta - \frac{\pi}{2} + \alpha$$

so that

$$I_{e1} = \frac{C_0}{a^{1.3}} \int_{\alpha - \pi/2}^{\beta - \pi/2 + \alpha} (\cos w)^{0.3} dw$$

Since the maximum contribution of the integral occurs at $x = 0$ (closest approach of signal to the Sun), a Maclaurin's series expansion is used for the integrand:

$$f(w) \cong f(0) + w\left(\frac{df}{dw}\right)_0 + \frac{w^2}{2!}\left(\frac{d^2f}{dw^2}\right)_0 + \frac{w^3}{3!}\left(\frac{d^3f}{dw^3}\right)_0 + \cdots + \frac{w^n}{n!}\left(\frac{d^nf}{dw^n}\right)_0 + \cdots$$

with

$$f(w) = (\cos w)^{0.3}$$

$$f(0) = 1$$

$$\frac{df}{dw} = -0.3 \sin w(\cos w)^{-0.7}$$

$$\left(\frac{df}{dw}\right)_0 = 0$$

$$\frac{d^2f}{dw^2} = -0.3(\cos w)^{0.3} - 0.21 \sin^2 w(\cos w)^{-1.7}$$

$$\left(\frac{d^2f}{dw^2}\right)_0 = -0.3$$

$$\frac{d^3f}{dw^3} = -0.33 \sin w(\cos w)^{-0.7} - 0.357 \sin^3 w(\cos w)^{-2.7}$$

$$\left(\frac{d^3f}{dw^3}\right)_0 = 0$$

$$\frac{d^4f}{dw^4} = -0.33(\cos w)^{0.3} - 1.302 \sin^2 w(\cos w)^{-1.7} - 0.063 \sin^4 w(\cos w)^{-3.7}$$

$$\left(\frac{d^1 f}{dw^1}\right)_0 = 0.33$$

$$\frac{d^2 f}{dw^2} = -2.505 \sin w(\cos w)^{-0.7} - 6.069 \sin^3 w(\cos w)^{-2.7} - 3.566 \sin^5 w(\cos w)^{-4.7}$$

$$\left(\frac{d^3 f}{dw^3}\right) = 0$$

$$\frac{d^4 f}{dw^4} = 2.505(\cos w)^{0.3} - 19.9605 \sin^2 w(\cos w)^{-1.7} - 34.218 \sin^4 w(\cos w)^{-3.7} - 16.762 \sin^6 w(\cos w)^{-5.7}$$

$$\left(\frac{d^4 f}{dw^4}\right)_0 = 2.505$$

$$(\cos w)^{0.3} \cong 1 + \frac{w^2}{2!}(-0.3) + \frac{w^4}{4!}(-0.33) + \cdots = 1 - 0.15w^2 - 0.01375w^4 + \cdots$$

The desired quantity then becomes:

$$I_{e1} = \frac{C_0}{a^{1.3}} \int_{\alpha-\pi/2}^{\beta-\pi/2+\alpha} (\cos w)^{0.3}\, dw$$

$$= \frac{C_0}{a^{1.3}} \int_{\alpha-\pi/2}^{\beta-\pi/2+\alpha} (1 - 0.15w^2 - 0.01375w^4 + \cdots)\, dw$$

$$= \frac{C_0}{a^{1.3}} \left[w - \frac{0.15w^3}{3} - \frac{0.01375w^5}{5} + \cdots \right]_{\alpha-\pi/2}^{\beta-\pi/2+\alpha}$$

$$\cong \frac{C_0}{a^{1.3}} \left[w - 0.05w^3 - 0.00275w^5 \right]_{\alpha-\pi/2}^{\beta-\pi/2+\alpha}$$

$$= \frac{C_0}{a^{1.3}} [(\beta - \pi/2 + \alpha) - (\alpha - \pi/2) - 0.05\{(\beta - \pi/2 + \alpha)^3 - (\alpha - \pi/2)^3\} - 0.00275\{(\beta - \pi/2 + \alpha)^5 - (\alpha - \pi/2)^5\}]$$

$$= \frac{C_0 \beta}{a^{1.3}} \left[1 - 0.05 \left\{ \frac{(\beta - \pi/2 + \alpha)^3 - (\alpha - \pi/2)^3}{\beta} \right\} - 0.00275 \left\{ \frac{(\beta - \pi/2 + \alpha)^5 - (\alpha - \pi/2)^5}{\beta} \right\} \right]$$

Defining:

$$A_0 = \frac{C_0}{(r_e)^{1.3}}$$

one arrives at the final expression for I_{e1}:

$$I_{e1} = A_0 \left[\frac{\beta}{(\sin \alpha)^{1.3}} \right] F(\alpha,\beta)$$

where

$$F(\alpha,\beta) = 1 - 0.05 \left\{ \frac{(\beta - \pi/2 + \alpha)^3 - (\alpha - \pi/2)^3}{\beta} \right\} - 0.00275 \left\{ \frac{(\beta - \pi/2 + \alpha)^5 - (\alpha - \pi/2)^5}{\beta} \right\}$$

One now wishes to evaluate the C_1/r^6 term:

$$I_{e2} = C_1 \int_0^{R_{s/c}} \frac{dR}{r^6}$$

Using notation similar to the previous integral, one has:

$$I_{e2} = C_1 \int_{-r_e \cos\alpha}^{R_{s/c} - r_e \cos\alpha} \frac{dx}{(x^2 + a^2)^3}$$

$$= \frac{C_1}{a^6} \int_{-r_e \cos\alpha}^{R_{s/c} - r_e \cos\alpha} \frac{dx}{\left(1 + \frac{x^2}{a^2}\right)^3}$$

$$= \frac{C_1}{a^6} \int_{\tan^{-1}\frac{(-r_e \cos\alpha)}{a}}^{\tan^{-1}\frac{(R_{s/c} - r_e \cos\alpha)}{a}} \frac{a \sec^2 w\, dw}{(\tan^2 w + 1)^3}$$

$$= \frac{C_1}{a^5} \int_{\alpha-\pi/2}^{\beta-\pi/2+\alpha} \frac{dw}{(\tan^2 w + 1)^2}$$

$$= \frac{C_1}{a^5} \int_{\alpha-\pi/2}^{\beta-\pi/2+\alpha} (\cos w)^4\, dw$$

which simply yields

$$I_{e2} = \frac{C_1}{a^5} \left[\frac{3}{8} w + \frac{1}{4} \sin 2w + \frac{1}{32} \sin 4w \right]_{\alpha-\pi/2}^{\beta-\pi/2+\alpha}$$

Because of the $(1/a^5)$ dependency, one only needs to consider the case:

$$\alpha \to 0$$
$$\beta \to \pi$$

Let

$$\alpha \equiv \Delta_\alpha \qquad \Delta_\alpha > 0$$
$$\beta \equiv \pi - \Delta_\beta \qquad \Delta_\beta > 0$$

One then has:

$$I_{e2} = \frac{C_1}{a^5}\left[\frac{3}{8}\{\beta - \pi/2 + \alpha - (\alpha - \pi/2)\} + \frac{1}{4}\{\sin[2(\alpha+\beta) - \pi] - \sin[2\alpha - \pi]\} + \frac{1}{32}\{\sin[4(\alpha+\beta) - 2\pi] - \sin[4\alpha - 2\pi]\}\right]$$

$$= \frac{C_1}{a^5}\left[\frac{3}{8}\beta + \frac{1}{4}\{\sin[\pi + 2(\Delta_\alpha - \Delta_\beta)] + \sin[\pi - 2\Delta_\alpha]\} + \frac{1}{32}\{\sin[2\pi + 4(\Delta_\alpha - \Delta_\beta)] + \sin[2\pi - 4\Delta_\alpha]\}\right]$$

Now

$$\sin[\pi + 2(\Delta_\alpha - \Delta_\beta)] \approx -2(\Delta_\alpha - \Delta_\beta)$$
$$\sin[\pi - 2\Delta_\alpha] \approx +2\Delta_\alpha$$
$$\sin[2\pi + 4(\Delta_\alpha - \Delta_\beta)] \approx +4(\Delta_\alpha - \Delta_\beta)$$
$$\sin[2\pi - 4\Delta_\alpha] \approx -4\Delta_\alpha$$

so that

$$I_{e1} = \frac{C_1}{a^5}\left[\frac{3}{8}\beta + \frac{1}{4}\{-2(\Delta_\alpha - \Delta_\beta) + 2\Delta_\alpha\} + \frac{1}{32}\{4(\Delta_\alpha - \Delta_\beta) - 4\Delta_\alpha\}\right]$$

$$= \frac{C_1}{a^5}\left[\frac{3}{8}\beta + \frac{4}{8}\Delta_\beta - \frac{1}{8}\Delta_\beta\right]$$

$$= \frac{C_1}{a^5}\left[\frac{3}{8}(\beta + \Delta_\beta)\right]$$

$$= \frac{C_1}{a^5}\left[\frac{3\pi}{8}\right]$$

Defining

$$A_1 = \frac{C_1}{(r_e)^5}\left[\frac{3\pi}{8}\right]$$

one has

$$I_{e2} = \frac{A_1}{(\sin\alpha)^5}$$

The model ISED (integrated solar electron density) is thus defined:

$$\text{ISED} = I_{e1} + I_{e2} = A_0\left[\frac{\beta}{(\sin\alpha)^{1.3}}\right]F(\alpha,\beta) + A_1\left[\frac{1}{(\sin\alpha)^5}\right]$$

with

$$F(\alpha,\beta) = 1 - 0.05\left\{\frac{(\beta - \pi/2 + \alpha)^3 - (\alpha - \pi/2)^3}{\beta}\right\} - 0.00275\left\{\frac{(\beta - \pi/2 + \alpha)^5 - (\alpha - \pi/2)^5}{\beta}\right\}$$

It is noteworthy to compare the above formulation with the NOISE_p model, which is in good agreement with the doppler noise observations presented in Refs. 1, 6, and 7:

$$\text{NOISE}_p = K_0\frac{\beta^{1.29}}{(\sin\alpha)^{1.29}}$$

Recall that the original hypothesis in Ref. 1 $(1/r^2$ dependency) led to the dominant variable:

$$\sim \frac{1}{\sin\alpha}$$

and that to obtain a better fit to the doppler noise observations, it was necessary to (empirically) adjust the power of the dominant variable:

$$\sim \frac{1}{(\sin\alpha)^{1.29}}$$

which is now seen to be in almost perfect agreement with the dominant variable in the first term of the ISED formulation. That an empirically adjusted model would prove to be in excellent (functional) correspondence with the actual electron content along the signal path (ISED), would certainly argue persuasively in favor of strong correlation between observed doppler noise and ISED. Addi-

tionally, this result should not be surprising, as it was certainly alluded to by Muhleman, et al., in Ref. 5, p. 100: "The phase jitter essentially depends on the electron density fluctuation, and the observing wavelength and the density fluctuations are approximately proportional to the mean density."

A further observation along these lines is provided by G. L. Dutcher, (Ref. 8, pp. 15–16), who also indicates that the electron density fluctuation is proportional to the mean electron density, and additionally, indicates the approximate constant of proportionality (p. 50):

$$\left[\frac{\text{electron density fluctuations}}{\text{mean electron density}}\right]_{RMS} \approx 0.02$$

The observed doppler noise data from 1975 Pioneer 10, Pioneer 11, Helios 1 (first) and Helios 1 (second) solar conjunctions, as presented in Refs. 1 and 7, were fit to the ISED model, thereby producing the following fit constants:

$$A_0 = 9.65 \times 10^{1}$$

$$A_1 = 5 \times 10^{10}$$

If the data were really representative of the electron density function, one would expect the ratio of the coefficients determined from the observed data (A_0, A_1) to be similar to the ratio of the coefficients presented by Muhleman in Ref. 5. Normalizing terms to one solar radii, Muhleman indicates two sets of coefficients (pp. 95–96):

$$A = 1.3 \times 10^{5}$$

$$B = 1.15 \times 10^{6}$$

$$\frac{A}{B} = 113$$

and

$$A = 0.8 \times 10^{5}$$

$$B = 0.51 \times 10^{6}$$

$$\frac{A}{B} = 157$$

For the ISED case (normalized to one solar radius):

$$A_1' = C_1[r_e \sin(0.27°)]^{-6}$$

$$A_0' = C_0[r_e \sin(0.27°)]^{-2.3}$$

$$\frac{A_1'}{A_0'} = \frac{C_1[r_e \sin(0.27°)]^{2.3}}{C_0[r_e \sin(0.27°)]^{6}}$$

$$= \left(\frac{C_1}{C_0}\right)\frac{1}{[r_e \sin(0.27°)]^{3.7}}$$

$$= \frac{A_1(r_e)^5\left(\frac{8}{3\pi}\right)}{A_0(r_e)^{1.3}}\frac{1}{[r_e \sin(0.27°)]^{3.7}}$$

$$= \frac{A_1\left(\frac{8}{3\pi}\right)}{A_0[\sin(0.27°)]^{3.7}}$$

$$= 179$$

It is reassuring that the ratio of the coefficients determined from the observed doppler noise data is similar to the ratio of the coefficients determined from other experimental observations.

As in Ref. 7, all comparisons of observed doppler noise (N_1) to the various proposed models will be cast in logarithmic form, or dB:

$$\text{Doppler noise residual, } dB \equiv 10 \log_{10}\left(\frac{N_1}{\text{MODEL}}\right)$$

Using this standard, the statistics for the combined data base (in excess of 500 "pass average" doppler noise observations), when fit to the ISED model, were as follows:[2]

	PN 10	PN 11	HEL-1st	HEL-2nd	All
σ (dB)	1.88	1.91	2.07	2.00	1.95
Bias (dB)	+0.06	−0.45	+0.54	+0.38	0.00

Scatter diagrams (observed noise vs the ISED model) can be seen in Appendix A as follows:

Fig. A1—Pioneer 10

Fig. A2—Pioneer 11

Fig. A3—Helios 1 first

Fig. A4—Helios 1 second

Fig. A5—Combined

[2]The standard deviation given by Muhleman (Ref. 5, p. 95) for the B term (0.51×10^6) is 0.30×10^6, or 2.15 dB, which is curiously similar to these numbers!

Qualitatively, the improvement of the ISED model over the previous $NOISE_p$ model can be seen by comparing the above figures to (respectively):

Fig. 8, Ref. 1

Fig. 9, Ref. 1

Fig. 10, Ref. 1

Fig. 7, Ref. 1

Fig. 3, Ref. 7

Improvement is most notably seen at very small SEPs and small ESPs. This is most probably a direct result of the following deficiencies in the previous $NOISE_p$ model:

(1) Lack of a $(\sin \alpha)^{-5}$ term (only applicable for SEP $\leq 1.5°$)

(2) $\beta^{1.29}$ versus the (correct) β.

Comparisons of the observed doppler noise versus the ISED model, as a function of day of year (DOY), are seen in Appendix B. Presentations are as follows:

Fig. B1—Pioneer 10

Fig. B2—Pioneer 11

Fig. B3—Helios 1 first

Fig. B4—Helios 1 second

Finally, the Muhleman Phase Jitter Model (from Ref. 5, Fig. 8, p. 100) has been frequently discussed and has always been found too small by an order of magnitude or more. What was not readily apparent was that the Muhleman model, as a function of the geometry, agrees with the observed doppler noise, except for a multiplicative constant! The following gives an approximate comparison of the ISED model and the Muhleman doppler phase jitter prediction:

SEP, deg	Muhleman model, Hz, one-way	ISED, Hz, two-way	Ratio ISED/ Muhleman
15.6	2.65×10^{-4}	1.33×10^{-2}	50
10.5	4.50×10^{-4}	2.27×10^{-2}	50
5.3	1.08×10^{-3}	5.60×10^{-2}	52
2.7	2.65×10^{-3}	1.34×10^{-1}	51
1.1	1.33×10^{-2}	6.60×10^{-1}	50

As can readily be seen, the models are extremely similar, when considered as a function of the geometry.

III. Correlation With Solar Activity: The RISED Model

In the previous section, observed doppler noise was modeled as a function of signal path electron content. However, as has already been pointed out in Refs. 6 and 7, systematic, cyclical deviations from the model appear when the residuals are viewed as a function of DOY. Additionally, these deviations display good correlation between different spacecraft, when the spacecraft signal paths are on the same side of the Sun (Ref. 7). Appendix C presents observed doppler noise residuals (in *dB*) from the ISED model as follows:

Fig. C1—Pioneer 10

Fig. C2—Pioneer 11

Fig. C3—Helios 1 first

Fig. C4—Helios 1 second

The question now arises, can observations of solar activity be used in some way to modify the ISED model and thus perhaps account for (in some fashion) the observed cyclical fluctuations about the ISED model? It is already well known that the electron density function fluctuates with the long-term solar cycle. For instance, Van De Hulst (Ref. 3) scales his electron density function by location within the solar cycle, with the maximum value approximately twice the minimum. Similarly, M. Waldmeier (Ref. 9) states: "For any heliographic latitude the electron density function is higher during sunspot maximum than during the minimum."

The ISED residuals seen in Appendix C frequently differ by 3 to 6 *dB* between neighboring maxima/minima. This would seem to be consistent with other observations of temporal changes in electron density; for instance, Dutcher (Ref. 8, p. 40) comments on changes by a factor of three (4.8 *dB*) over a period of days. Additionally, T. A. Croft, in Ref. 10, reports on variations of electron density which reappear approximately coincident with the solar rotation rate (p. 521): "The 27-day repetition is clearly seen in interplanetary electron content measurements obtained by the radio propagation experiment on the Pioneer spacecraft. . . . The measured electron content of the solar wind in mid-1970 exhibited a region of relatively high electron density that reappeared at intervals of about 27.8 days."

Considering the above, it was concluded that possibly the daily (Earth) observed Sunspot index (Zurich, R_Z) could be used in some fashion to adjust the ISED model and thereby attempt to lessen the magnitude of the systematic deviations of the observed doppler data from the model. If such a process were successfully executed, correlation could be demonstrated in a quantitative sense via a comparison to the previously presented ISED residual standard deviations (σ). To attempt this procedure, two separate aspects of the problem were addressed:

(1) *Phase.* An algorithm would be required to link in some internally consistent fashion the earth observation of solar activity, and the subsequent (or prior) effect on observed doppler noise.

(2) *Magnitude.* A function of R_Z would have to be empirically constructed to "scale" the ISED model.

The strongest correlation appeared to be between periods of zero sunspot activity and periods of very negative ($-3 \sim -4$ *dB*) residuals. Consideration of the time relationships between the two led to the following (strictly empirical) hypothesis (with the geometry as shown in Fig. 2).

Assume

(1) Each daily R_Z measurement is time centered (averaged) for a solar longitude = 0 deg.

(2) Variations in electron density "propagate" outward in a radial direction and at a constant speed (V_0) from a surface or corotating near surface region.

The above allows one to construct a consistent (but arbitrary) method of relating Earth observations of solar activity and signal path observations, as follows:

(1) Time to propagate from surface to signal closest approach:

$$t_\tau = \frac{1}{V_0}\{r_e \sin\alpha\}$$

$$= A_2 \sin\alpha$$

$$\cong A_2\alpha$$

(2) Time to rotate from Earth observation (0 deg longitude) to longitude of propagation region ($\gamma = \pi/2 - \alpha$ and ω_s = solar rotation period):

$$t_r = \frac{\omega_s}{2\pi}(\pm\gamma)\begin{cases} + \text{ signal west of Sun} \\ - \text{ signal east of Sun} \end{cases}$$

$$= \pm\frac{\omega_s}{2\pi}\left(\frac{\pi}{2} - \alpha\right)$$

$$\approx \pm\frac{27 \text{ days/rev}}{2\pi}\left(\frac{\pi}{2} - \alpha\right)$$

$$= \pm\left[6^{3}/_{4} - \frac{13.5}{\pi}\alpha\right]$$

Adding the two times together, one has

(1) West side

$$T = t_\tau + t_r = 6^{3}/_{4} + \alpha\left(A_2 - \frac{13.5}{\pi}\right)$$

(2) East side

$$T = t_\tau + t_r = -6^{3}/_{4} + \alpha\left(A_2 + \frac{13.5}{\pi}\right)$$

Finally, since the sunspot observations are a function of DOY, the phase time T is rounded to the nearest integer day:

$$n_t(\text{days}) \equiv \text{integer}\,(T + 0.5) \qquad T \geq 0$$

$$n_t(\text{days}) \equiv \text{integer}\,(T - 0.5) \qquad T < 0$$

The sunspot data are published as a function of DOY:

$$R_Z(\text{DOY})$$

Since the data exhibit sharp day to day fluctuations in addition to the longer term, higher magnitude fluctuations that are the primary concern here, the sunspot data were smoothed in the following manner:

$$YR_Z(\text{DOY}) = 0.1R_Z(\text{DOY} - 2) + 0.2R_Z(\text{DOY} - 1) + 0.4R_Z(\text{DOY}) + 0.2R_Z(\text{DOY} + 1) + 0.1R_Z(\text{DOY} + 2)$$

The smoothed phased sunspot value for a doppler noise observation on a given day (DOY) then becomes:

$$XR_Z(\text{DOY}) = YR_Z(\text{DOY} - n_t)$$

Finally, it was necessary to construct a function of XR_Z which could be used to scale the ISED model. Examination of the ISED residuals and the (phased) sunspot data

indicated a multiplicative function with the following general characteristics:

Sunspot activity (R_Z)	Multiplicative Characteristic
$0 \sim 10$	$\sim$0.5 for zero sunspots; quickly rising to about 1.0
$10 \sim 40$	>1.0 and very gradually increasing
$40 \sim 100$	gradually accelerating rate until $\sim$4.0 for 100 sunspots

To accomplish this, the following function was constructed:

$$WR_Z = (1 + A_4 XR_Z)(1 + A_5[XR_Z]^2) - A_6 \cos\left[\frac{\pi}{2}\left(\frac{XR_Z}{A_7 + XR_Z}\right)\right]$$

thus leading to the RISED (rotating integrated solar electron density) model, fully defined as follows:

$$\text{RISED} = WR_Z\left\{A_0\left[\frac{\beta}{(\sin\alpha)^{1.3}}\right]F(\alpha,\beta) + A_1\left[\frac{1}{(\sin\alpha)^5}\right]\right\}$$

with

$$F(\alpha,\beta) = 1 - 0.05\left\{\frac{(\beta - \pi/2 + \alpha)^3 - (\alpha - \pi/2)^3}{\beta}\right\} - 0.00275\left\{\frac{(\beta - \pi/2 + \alpha)^5 - (\alpha - \pi/2)^5}{\beta}\right\}$$

$$WR_Z = (1 + A_4 XR_Z)(1 + A_5[XR_Z]^2) - A_6 \cos\left[\frac{\pi}{2}\left(\frac{XR_Z}{A_7 + XR_Z}\right)\right]$$

$$XR_Z(\text{DOY}) = YR_Z(\text{DOY} - n_t)$$

$$YR_Z(\text{DOY}) = 0.1R_Z(\text{DOY} - 2) + 0.2R_Z(\text{DOY} - 1) + 0.4R_Z(\text{DOY}) + 0.2R_Z(\text{DOY} + 1) + 0.1R_Z(\text{DOY} + 2)$$

and

$$n_t = \begin{cases} \text{integer}\,(T + 0.5) & T \geq 0 \\ \text{integer}\,(T - 0.5) & T < 0 \end{cases}$$

where

$$T = \begin{cases} 6\tfrac{3}{4} + \alpha\left(A_2 - \dfrac{13.5}{\pi}\right) & \text{signal paths west of Sun} \\ -6\tfrac{3}{4} + \alpha\left(A_2 + \dfrac{13.5}{\pi}\right) & \text{signal paths east of Sun} \end{cases}$$

The observed doppler noise data from the Pioneer 10, Pioneer 11 and the Helios 1 first 1975 solar conjunctions, subject to the following (minor) restrictions: (1) data < 30 deg heliographic latitude (the signal closest approach point) and (2) data such that ISED > 0.003 Hz were fit to the RISED model, with the various A_n parameters varied to minimize the standard deviation of the residuals. This process yielded the following set of parameters:

$$A_0 = 9.153 \times 10^{-3}$$
$$A_1 = 1.2 \times 10^{-9}$$
$$A_2 = 1.2 \times 10^{+1}$$
$$A_4 = 9 \times 10^{-3}$$
$$A_5 = 1 \times 10^{-4}$$
$$A_6 = 4 \times 10^{-1}$$
$$A_7 = 5 \times 10^{-1}$$

The function WR_Z with the above A_4 through A_7 is plotted versus R_Z in Fig. 3. The statistics resulting from the determined parameter set were as follows:

	σ (dB)	Bias (dB)
Pioneer 10 east	1.58	+0.36
Pioneer 10 west	1.34	+0.18
Pioneer 11 east	1.57	−1.23
Pioneer 11 west	1.31	−0.17
Helios 1 first (west)	2.06	+0.44
Combined	1.55	0.00

By comparing these results to those obtained for the ISED case, a very substantial decrease in the (combined) standard deviation can be seen:

$\sigma = 1.86$ ISED[3]

$\sigma = 1.55$ RISED[3]

Basically, the RISED model very substantially improved the Pioneer 10 and Pioneer 11 results, (i.e., de-

creased the systematic deviations) and essentially left the Helios 1 (first) results unchanged. If only the (combined) Pioneer 10 and 11 results are compared, the improvement is even more dramatic:

$\sigma = 1.81$ ISED[3]

$\sigma = 1.38$ RISED[3]

A qualitative view of the improvement can be seen in Appendix C, where the following parameters are plotted as a function of DOY:

ISED residuals, *dB*

Smoothed, phased sunspots, XR_Z

RISED residuals, *dB*

and for the following cases:

Fig. C1—Pioneer 10

Fig. C2—Pioneer 11

Fig. C3—Helios 1 first

Additionally, Appendix D presents the observed doppler noise and the RISED model versus DOY for the following cases:

Fig. D1—Pioneer 10

Fig. D2—Pioneer 11

Fig. D3—Helios 1 first

while Appendix E presents the observed doppler noise versus the RISED model for the following cases:

Fig. E1—Pioneer 10

Fig. E2—Pioneer 11

Fig. E3—Helios 1 first

Fig. E4—Composite

When the Helios 1 second solar conjunction doppler noise data were fit to the RISED model with the fit parameters as previously determined, the results were quite disappointing—the RISED case producing a standard deviation very substantially worse than for the ISED case. It was noted that there occurred an extremely sharp peak in (observed) sunspot activity on DOY 218, and a correspondingly sharp peak in ISED residuals on DOY 234. Assuming that these events should correlate, a (constant) delay factor in the phasing relationship was introduced:

$$T(\text{west}) = 6\tfrac{3}{4} + \alpha\left(A_2 - \frac{13.5}{\pi}\right) + A_3$$

A new A_0 and A_1 were selected, yielding the following fit parameter set:

$A_0 = 7.6 \times 10^{-4}$

$A_1 = 5 \times 10^{-10}$

$A_2 = 1.2 \times 10^{+1}$

$A_3 = 8.25$

$A_4 = 9 \times 10^{-3}$

$A_5 = 1 \times 10^{-4}$

$A_6 = 4 \times 10^{-1}$

$A_7 = 5 \times 10^{-1}$

The statistics for the RISED model with this parameter set, as compared to the ISED model results, were as follows:

Helios 1 second (west) $\sigma = 1.90$; RISED

Helios 1 second (east) $\sigma = 1.63$; RISED

Helios 1 second (all) $\sigma = 1.77$; RISED

Helios 1 second (all) $\sigma = 2.00$; ISED

The RISED residuals, ISED residuals, and the smoothed, phased sunspots can be seen in Fig. C4, Appendix C; while the RISED residuals and observed doppler noise data versus DOY are seen in Fig. D4, Appendix D.

Although the standard deviation is significantly reduced for this RISED fit when compared to the ISED case, little significance can be attached to it because of the major alteration required to the basic RISED algorithm. This negative experience in projecting the RISED model forward to a new set of solar conjunction data leads one to (negatively) consider:

(1) Additional, currently unknown factors will have to be considered before a doppler noise model can incorporate observed solar activity in a quantitative fashion.

[3]For the "slightly" reduced data set, as previously defined.

(2) As a practical matter, it may not be possible to incorporate observed solar activity into a doppler noise model in a quantitative fashion.

Regardless of this failure to successfully project the RISED model forward, it is felt that the experience of the RISED model with the Pioneer 10, Pioneer 11, and Helios 1 (first) Solar conjunction doppler noise data represents an extremely strong, quantitative indication of correlation between Earth-observed solar activity and (assumed) fluctuations in electron density.

IV. Applications of the ISED Model

Applications of the work done to date in analyzing the 1975 solar conjunction observed doppler noise would appear to separate into two distinct categories, these being:

(1) Applications which only require doppler noise to be modeled as an arbitrary function of Earth-Sun-probe geometry, and which already appear to have a strong likelihood of successful realization.

(2) Applications which require the central hypothesis of the functional relationship between observed doppler noise and the signal path integration of electron density to be established, and hence, are less certain in terms of a successful realization.

These will be briefly expounded upon below in Subsections A and B.

A. Expected Applications

1. Validation of doppler data generation during solar conjunction phases. With the current ISED model, the real-time Network Analysis Team, Tracking (NAT TRACK) has a standard against which doppler noise can be compared, and which can be used to separate out possible Tracking System malfunctions. In support of this effort, the Network Operations Analysis Group, Tracking (NOAG TRACK) is currently providing NAT TRACK with ISED plots for any spacecraft in solar conjunction.

2. Planning for critical mission operations during solar conjunction phases. The ISED model can be used to quantitatively establish minimum requirements and tradeoff factors for the planning of critical mission events within solar conjunction phases. For instance, as a function of time, one can easily compute:

$$\frac{d\text{ISED}}{dt} = \frac{\partial \text{ISED}}{\partial \alpha}\frac{d\alpha}{dt} + \frac{\partial \text{ISED}}{\partial \beta}\frac{d\beta}{dt}$$

where

$$\frac{\partial \text{ISED}}{\partial \alpha} \approx -\frac{1.3\, A_0 \beta\, F(\alpha,\beta)}{(\sin\alpha)^{2.3}}\cos\alpha - \frac{5\, A_1 \cos\alpha}{(\sin\alpha)^6}$$

$$\frac{\partial \text{ISED}}{\partial \beta} \approx \frac{A_0\, F(\alpha,\beta)}{(\sin\alpha)^{1.3}}$$

and where the quantities

$$\frac{d\alpha}{dt}, \frac{d\beta}{dt}$$

are easily obtainable from standard trajectory information. The rate of change of ISED with time could then be used quantitatively to establish tradeoffs of solar corruption of navigation data with other mission characteristics.

B. Possible Applications

1. Accurate measurement of long term (~months) average electron density levels. During any solar conjunction period, numerous measurements of doppler noise will be obtained, which when used in conjunction with the ISED model, might be expected to provide an accurate "average" electron density level.

2. Measurement of intermediate (~days/weeks) electron density fluctuations. Multiple doppler noise measurements per day combined with the ISED model might be expected to provide a reasonable measurement of intermediate fluctuations in the average electron density level.

3. Correlation of observed solar activity with fluctuations in electron density. The intermediate fluctuations in electron density might be expected to constitute a powerful tool in correlative studies of Earth observed solar activity (perhaps similar to the RISED effort).

V. Summary

This report suggests that observed doppler noise is a direct function of the total electron content along the signal path:

$$\text{doppler noise} = K\int_0^{R_{s/c}} N_e(r)dR$$

which directly leads to a geometrical model (ISED) for the prediction of doppler noise:

$$\text{ISED} = A_0\left[\frac{\beta}{(\sin\alpha)^{1.3}}\right]F(\alpha,\beta) + A_1\left[\frac{1}{(\sin\alpha)^5}\right]$$

$$F(\alpha,\beta) = 1 - 0.05\left\{\frac{(\beta - \pi/2 + \alpha)^3 - (\alpha - \pi/2)^3}{\beta}\right\}$$

$$- 0.00275\left\{\frac{(\beta - \pi/2 + \alpha)^5 - (\alpha - \pi/2)^5}{\beta}\right\}$$

A best fit of this model to the combined Pioneer 10, Pioneer 11, and Helios 1 1975 solar conjunction doppler noise produced the following fit parameters:

$$A_0 = 9.65 \times 10^{-4}$$

$$A_1 = 5 \times 10^{-10}$$

and a standard deviation about the ISED model of:

$$1\sigma = 2.0\,\text{dB}\ \{\text{factor of } 1.58\}$$

Attempts to correlate systematic deviations from the ISED model with observed solar activity (RISED) produced a substantial decrease in systematic model error (for a selected data set):

$$1\sigma = 1.6\,\text{dB}\ \{\text{factor of } 1.45\}$$

However, it was not possible to successfully project the RISED model forward to a new (Helios 1 second) data base.

Finally, certain benefits are expected to have strong likelihood of realization:

(1) Validation of doppler data generation during solar conjunction phases.

(2) Planning for future mission critical phases during solar conjunctions.

Additional, but far less certain, benefits may also accrue:

(1) Determination of long term (~months) electron density levels.

(2) Determination of intermediate (~days/weeks) fluctuations in electron density levels.

(3) Detailed electron density information (particularly of the inner corona) which might be useful in correlative studies of solar activity.

Acknowledgments

A hearty thanks is extended to two individuals who greatly aided in the bringing of this report to fruition: F. Almon, for her excellent rapid-fire typing, and M. Cates, for her pellucid eye-pleasing graphical illustrations.

References

1. Berman, A. L., and Rockwell, S. T., "Analysis and Prediction of Doppler Noise During Solar Conjunctions," in *The Deep Space Network Progress Report 42-30*, Jet Propulsion Laboratory, Pasadena, Calif., Dec. 15, 1975.

2. Efron, L., and Lisowski, R. J., "Charged Particle Effects to Radio Ranging and Doppler Tracking Signals in a Radially Outflowing Solar Wind," in Space Programs Summary 37-56, Volume II: *The Deep Space Network*, Jet Propulsion Laboratory, Pasadena, Calif., March 31, 1969.

3. Van De Hulst, J. C., "The Electron Density of the Solar Corona," *Bulletin of the Astronomical Institutes of the Netherlands*, Vol. XI, Number 410, Feb. 2, 1950.

4. Stelzried, C. T., *A Faraday Rotation Measurement of a 13 CM Signal in the Solar Corona*, Technical Report 32-1401, Jet Propulsion Laboratory, Pasadena, Calif., July 15, 1970.

5. Muhleman, D. O., Anderson, J. D., Esposito, P. B., and Martin, W. L., "Radio Propagation Measurements of the Solar Corona and Gravitational Field; Applications to Mariner 6 and 7," in *Proceedings of the Conference on Experimental Tests of Gravitational Theories*, California Institute of Technology, Pasadena, Calif., Nov. 1970.

6. Berman, A. L., and Rockwell, S. T., "Correlation of Doppler Noise During Solar Conjunction With Fluctuations in Solar Activity," in *The Deep Space Network Progress Report 42-30*, Jet Propulsion Laboratory, Pasadena, Calif., Dec. 15, 1975.

7. Berman, A. L., "Analysis of Solar Effects Upon Observed Doppler Data Noise During the Helios 1 Second Solar Conjunction," in *The Deep Space Network Progress Report 42-32*, Jet Propulsion Laboratory, Pasadena, Calif., April 15, 1976.

8. Dutcher, G. L., *A Communication Channel Model of the Solar Corona and the Interplanetary Medium*, CSRT-69-1, Center for Space Research, Massachusetts Institute of Technology, 1969.

9. Waldmeier, M., "Slow Variations in the Solar Corona," in *The Solar Corona*, edited by J. W. Evans, Academic Press, New York, 1963.

10. Croft, T. A., "Corotation of An Intermittent Solar Wind Source," in *Solar Wind*, edited by C. P. Sonett, P. J. Coleman, Jr., and J. M. Wilcox, Ames Research Center, National Aeronautics and Space Administration, Washington, D. C., 1972.

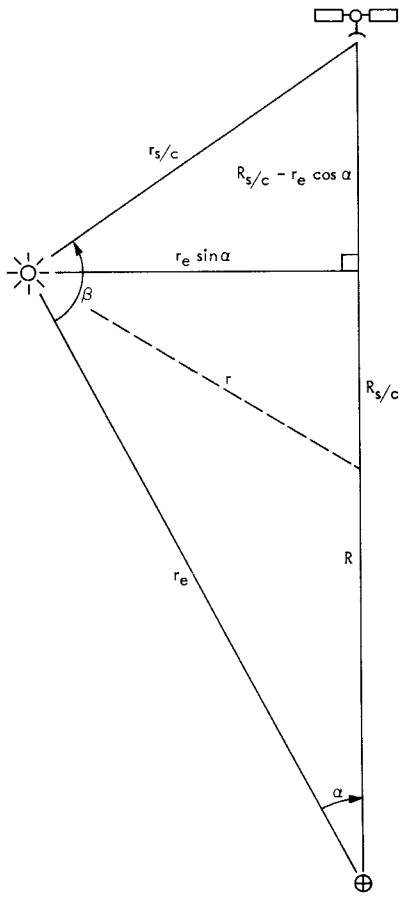

Fig. 1. Sun–Earth–spacecraft geometry

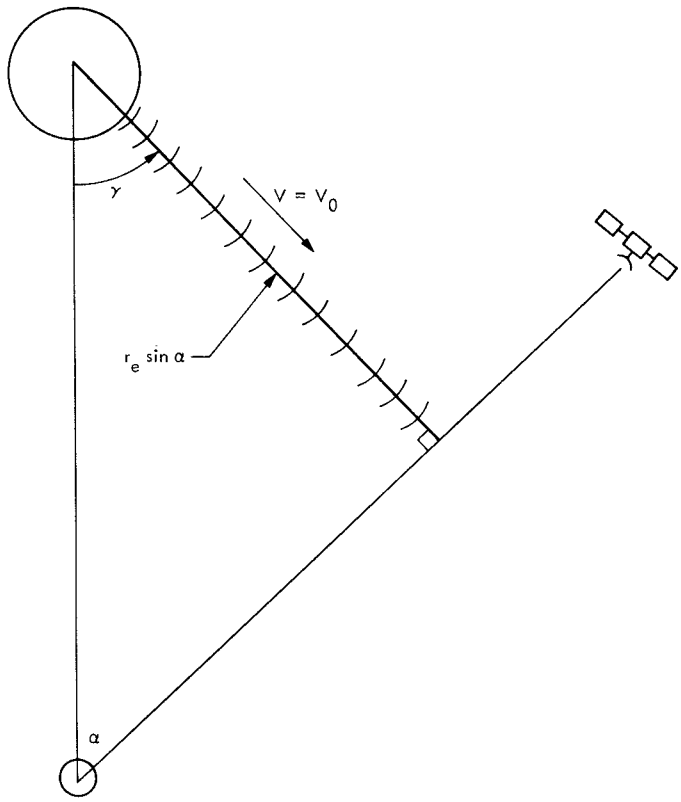

Fig. 2. Correlation phase geometry

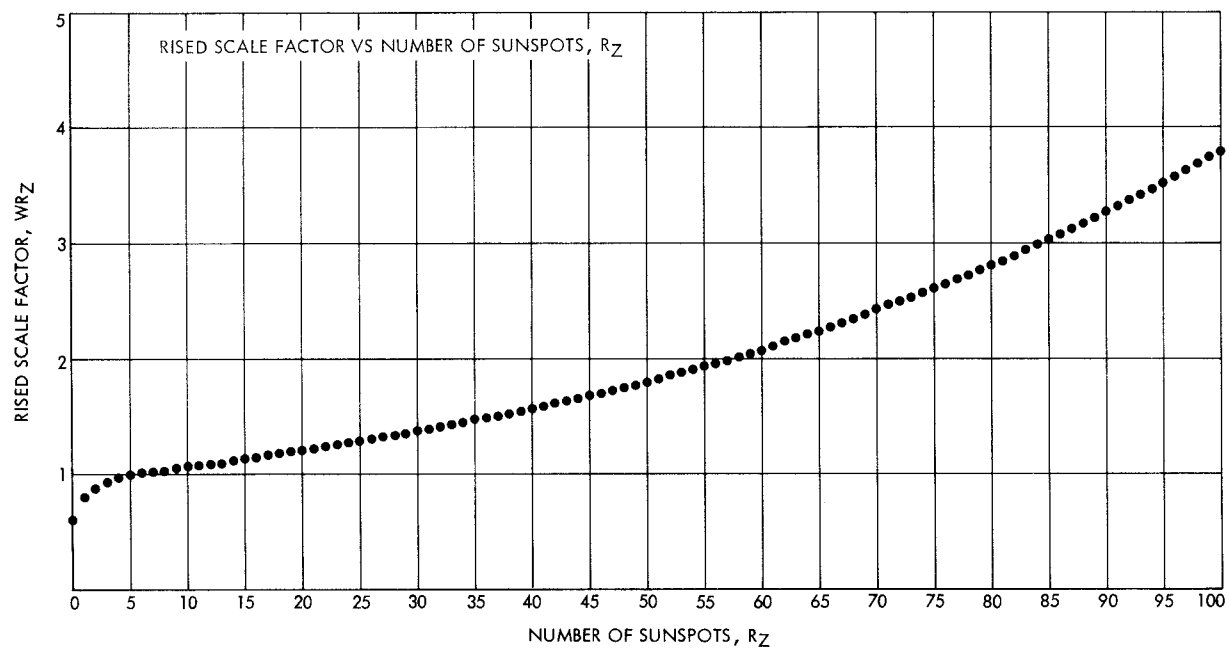

Fig. 3. RISED scale factor vs number of sunspots, R_Z

Appendix A

Observed Noise versus the ISED Model

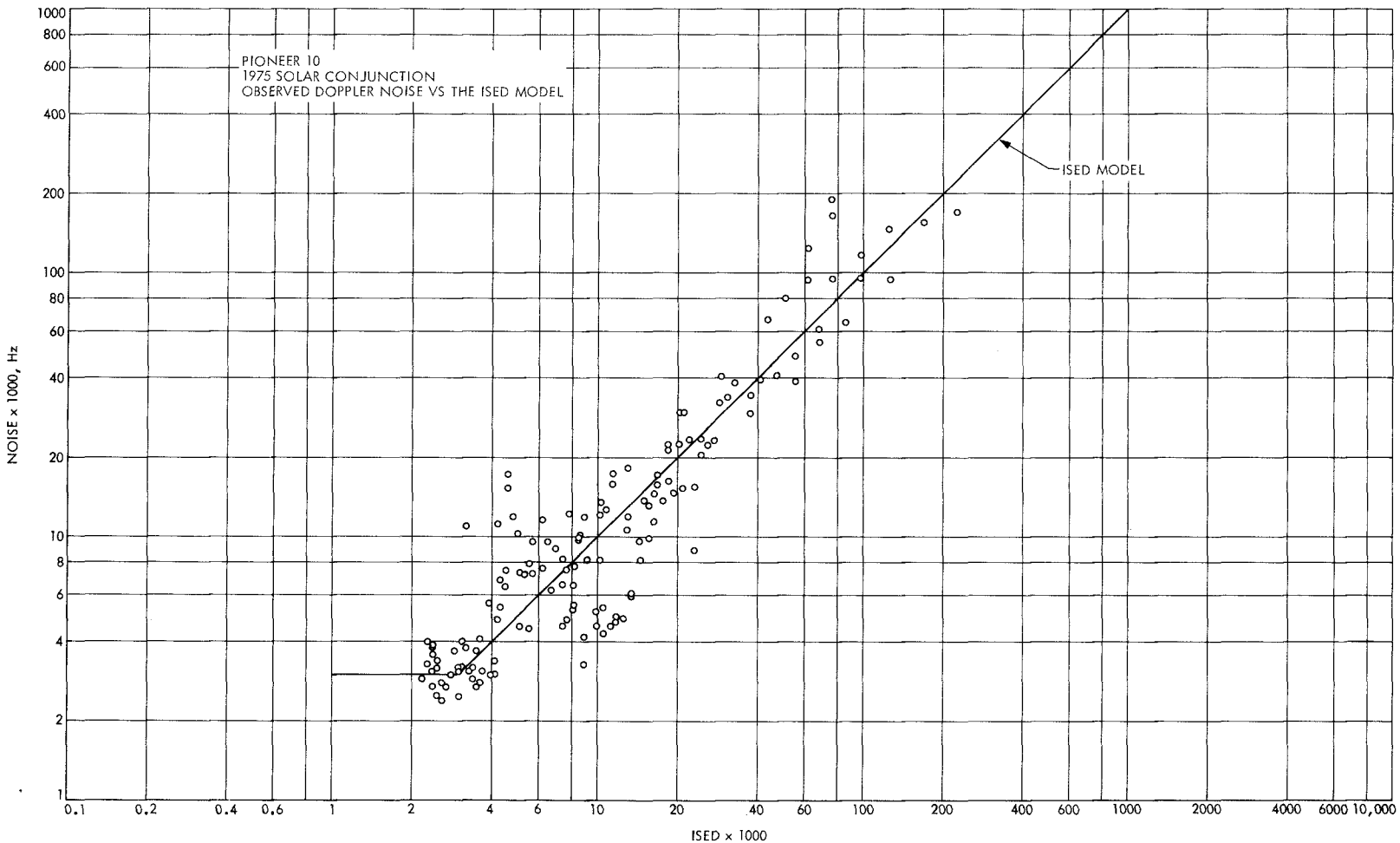

Fig. A-1. Pioneer 10 1975 solar conjunction observed doppler noise versus the ISED model

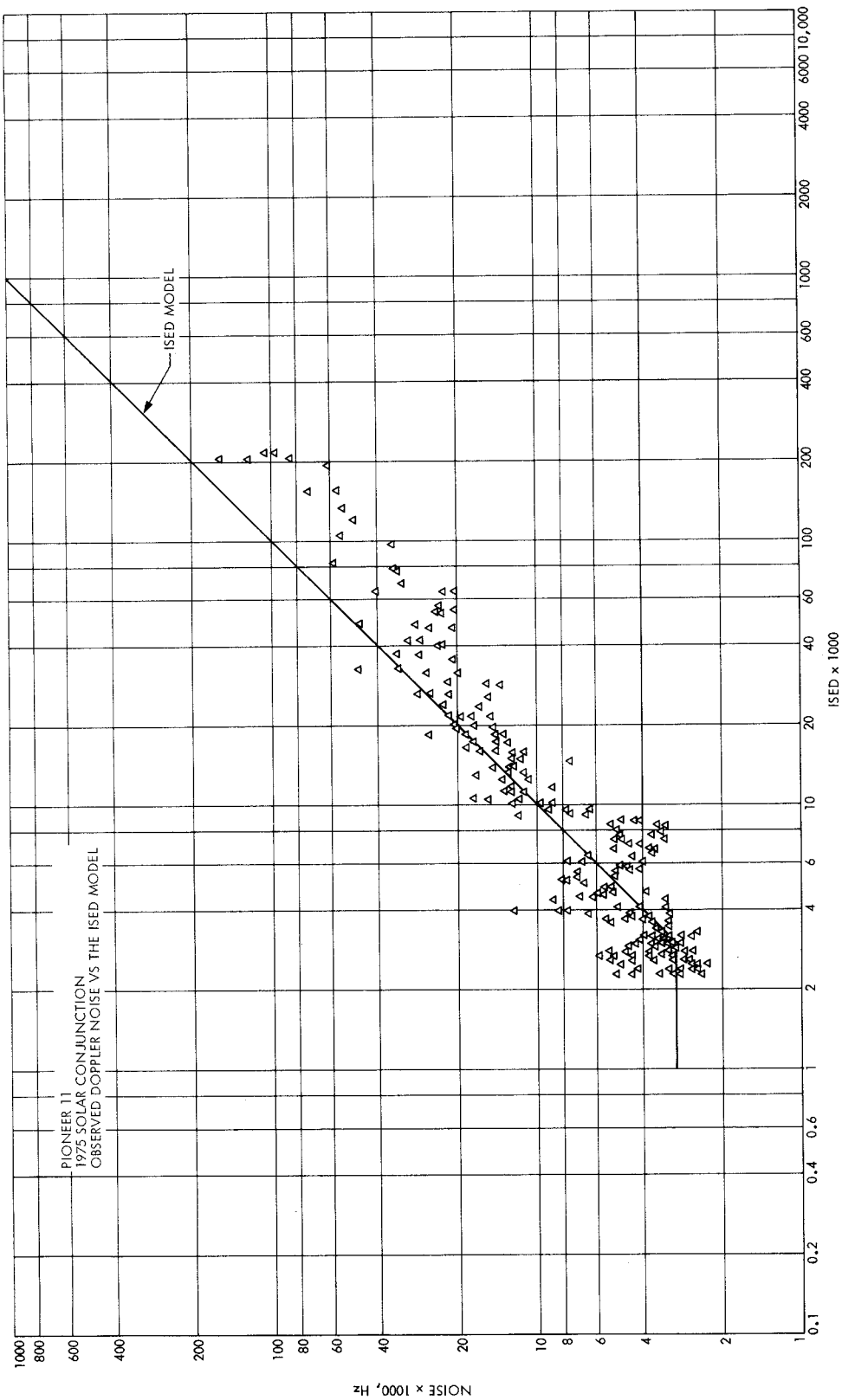

Fig. A-2. Pioneer 11 1975 solar conjunction observed doppler noise versus the ISED model

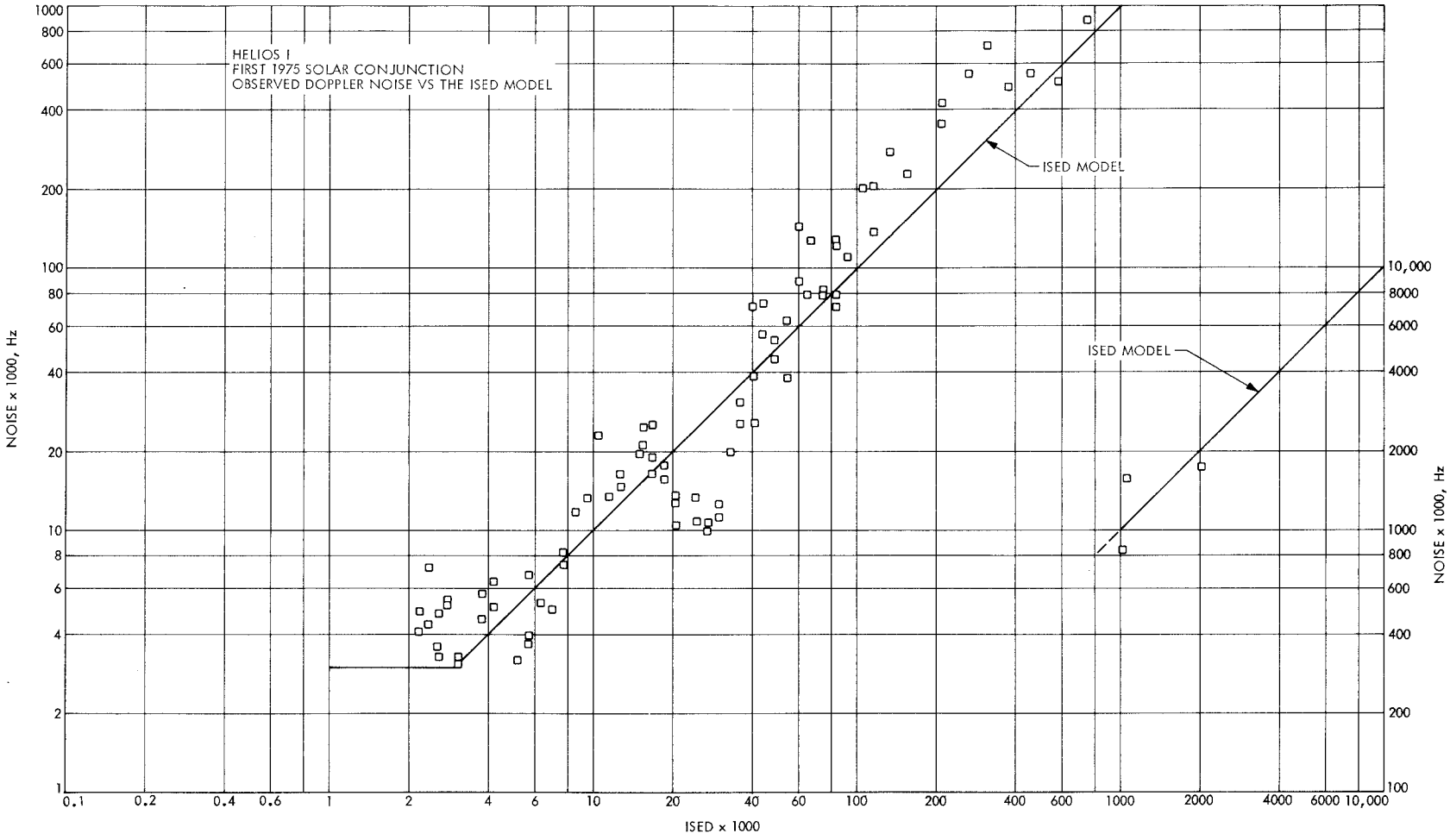

Fig. A-3. Helios 1 first 1975 solar conjunction observed doppler noise versus the ISED model

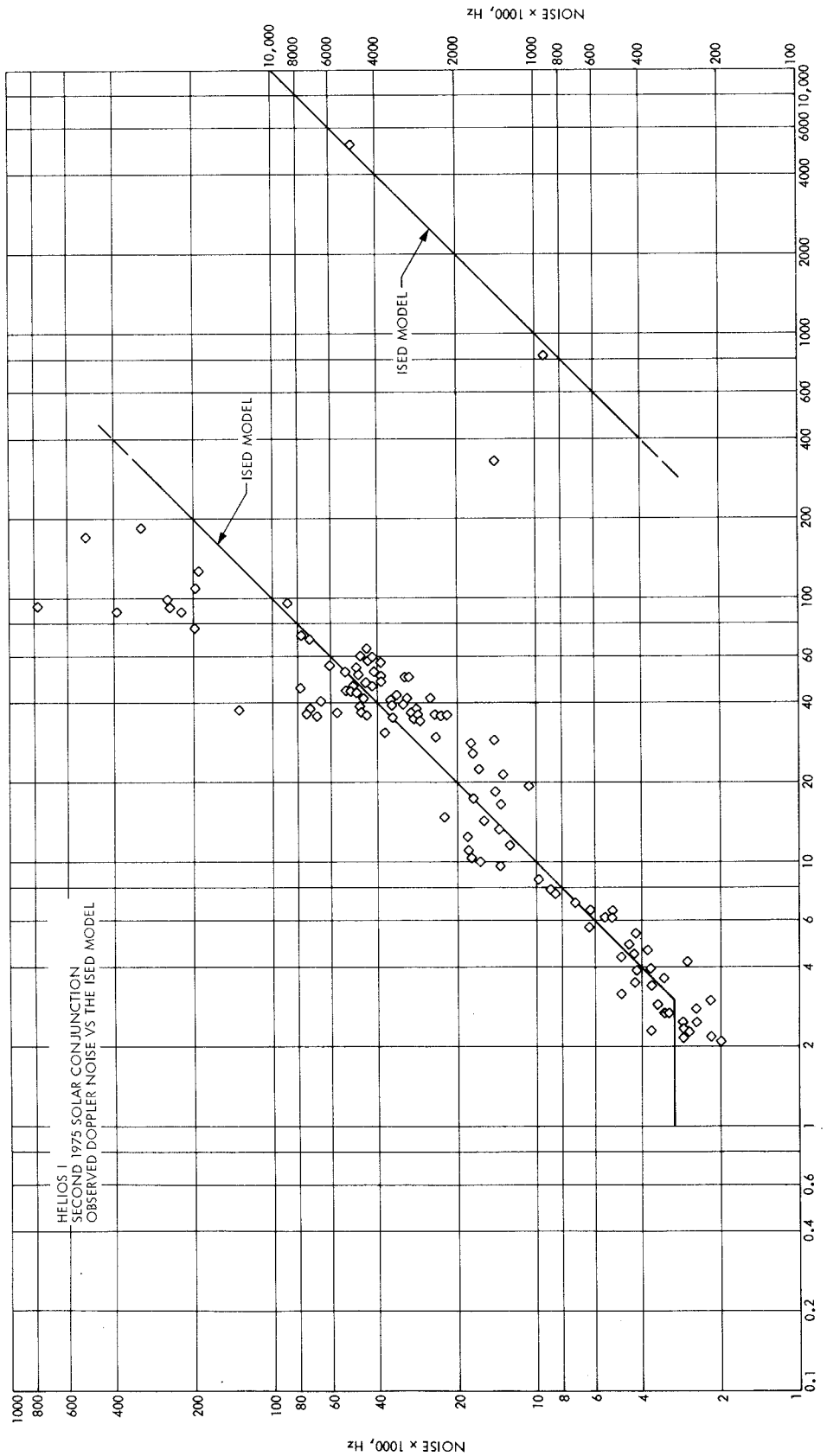

Fig. A-4. Helios 1 second 1975 solar conjunction observed doppler noise versus the ISED model

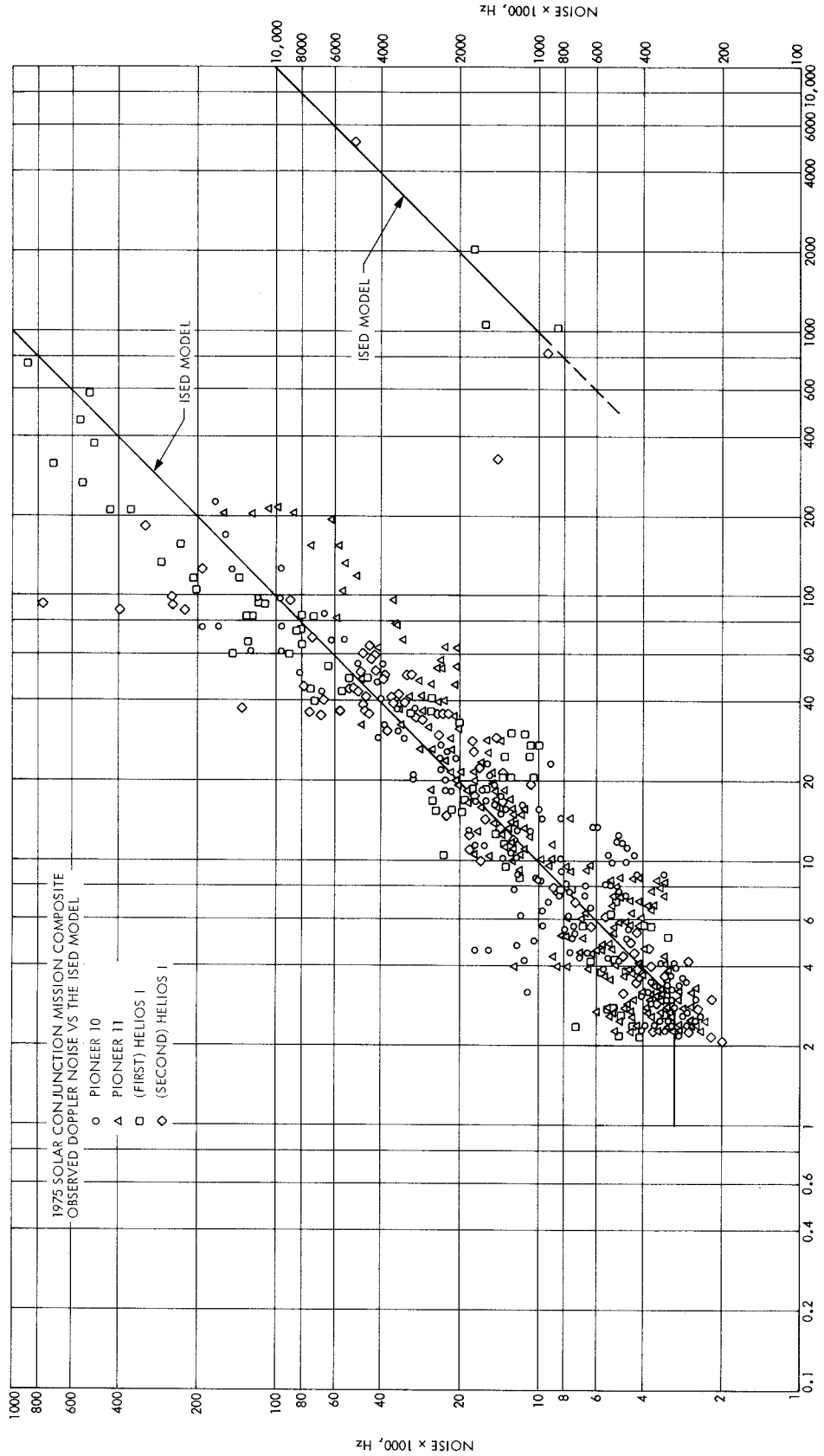

Fig. A-5. 1975 solar conjunction mission composite observed doppler noise versus the ISED model

Appendix B

Observed Noise and the ISED Model versus Day of Year

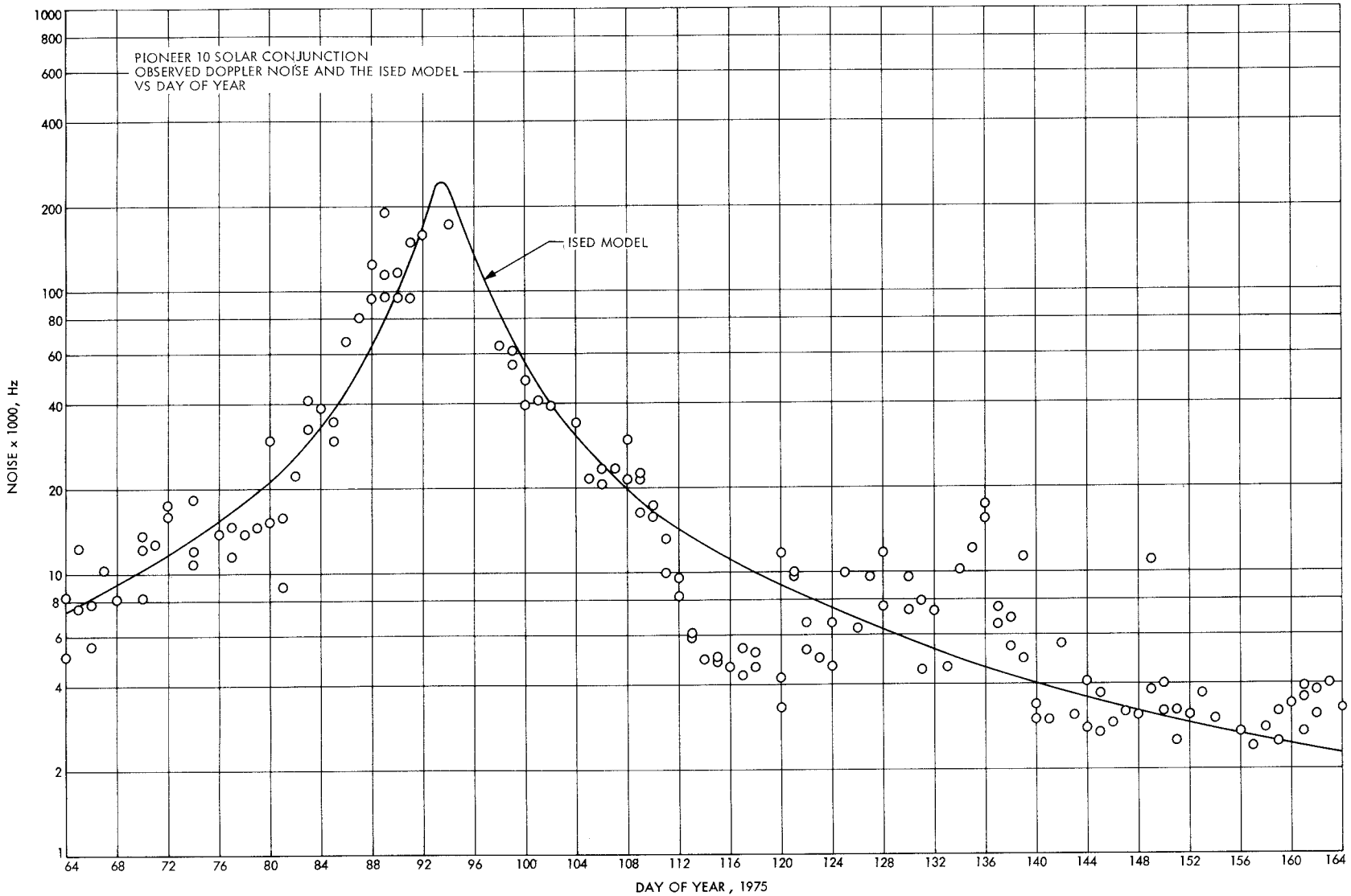

Fig. B-1. Pioneer 10 solar conjunction observed doppler noise and the ISED model versus day of year

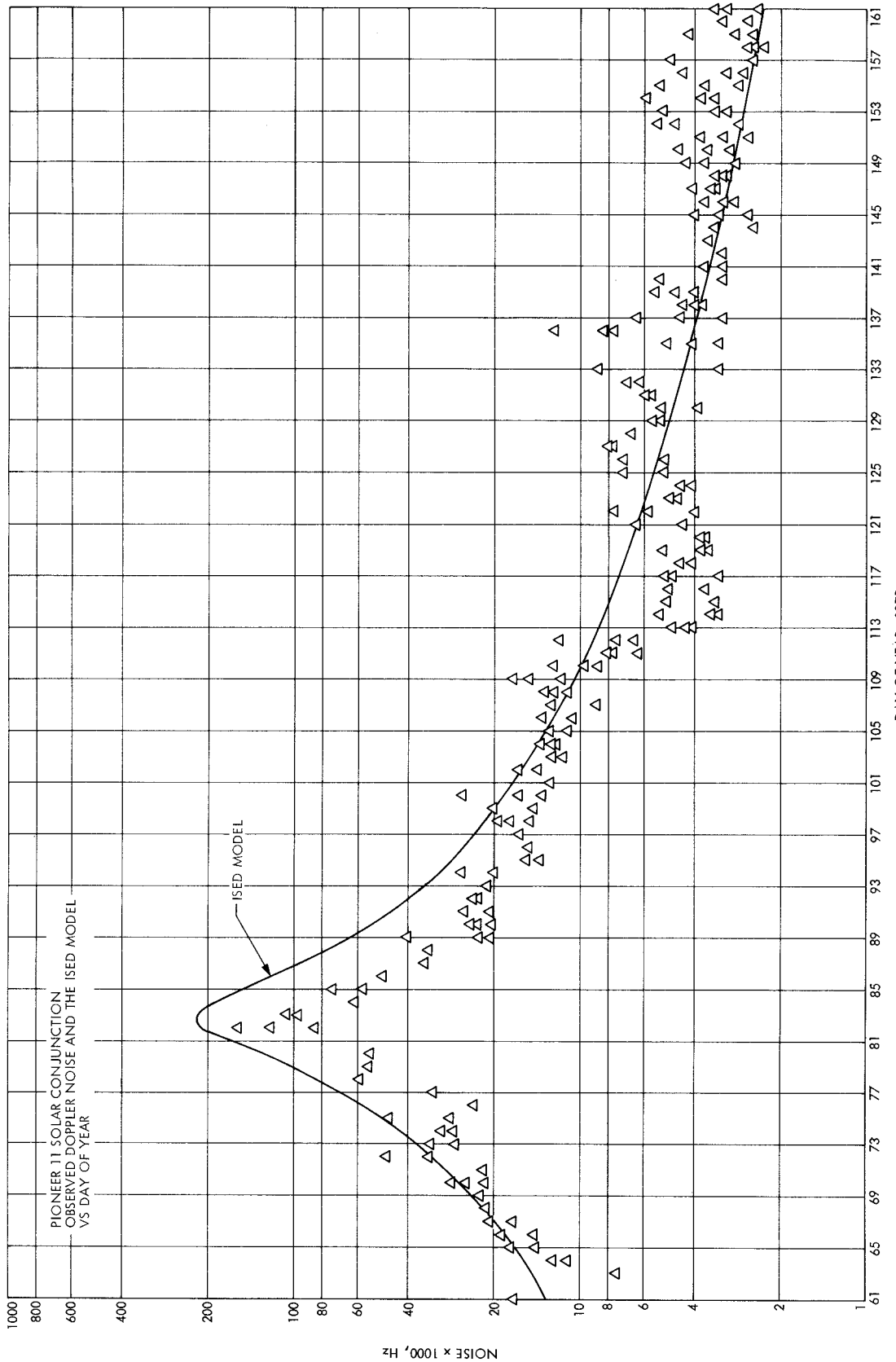

Fig. B-2. Pioneer 11 solar conjunction observed doppler noise and the ISED model versus day of year

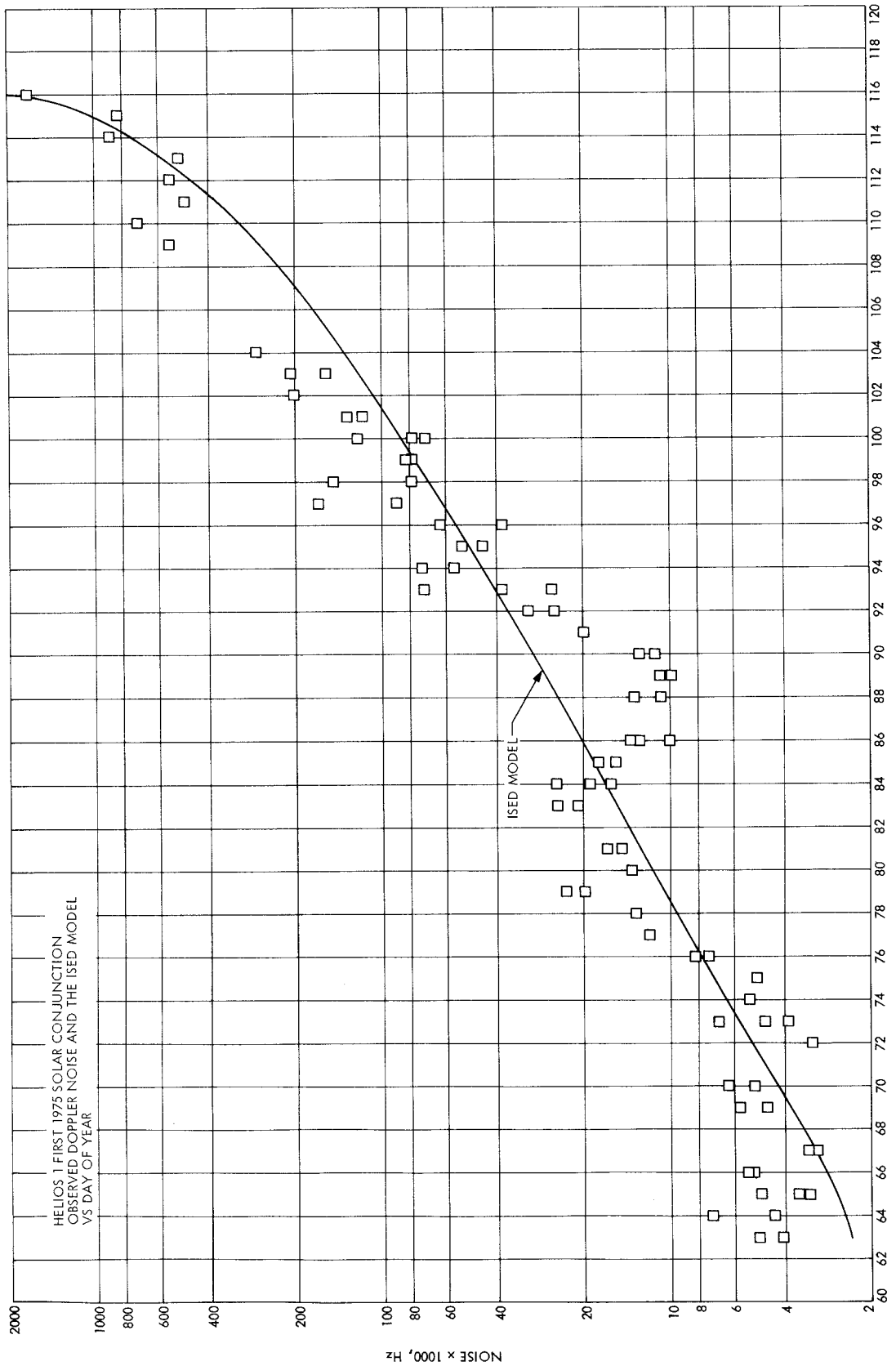

Fig. B-3. Helios 1 first 1975 solar conjunction observed doppler noise and the ISED model versus day of year

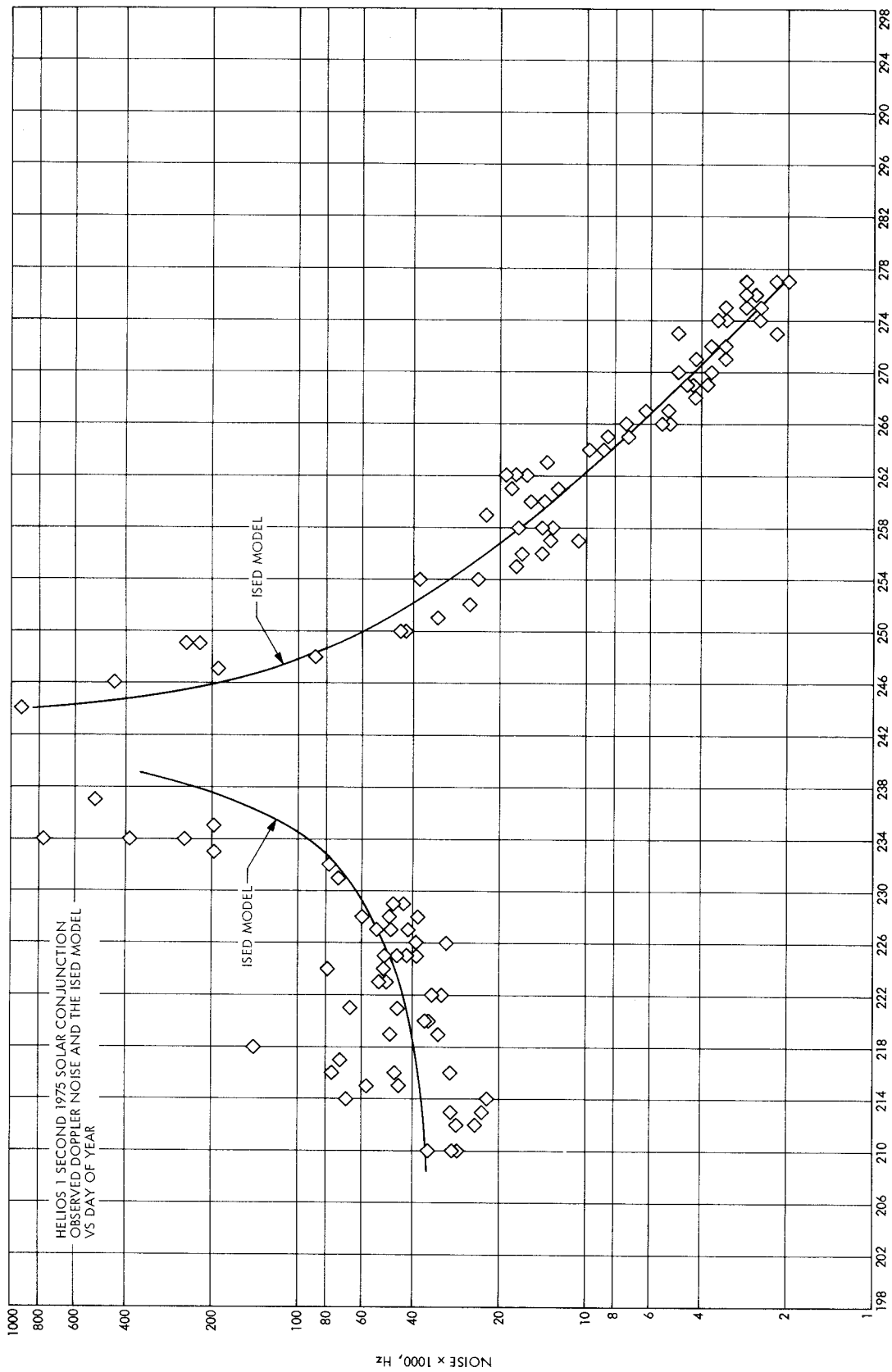

Fig. B-4. Helios 1 second 1975 solar conjunction observed doppler noise and the ISED model versus day of year

Appendix C

ISED Residuals, Smoothed/Phased Sunspots, and RISED Residuals versus Day of Year

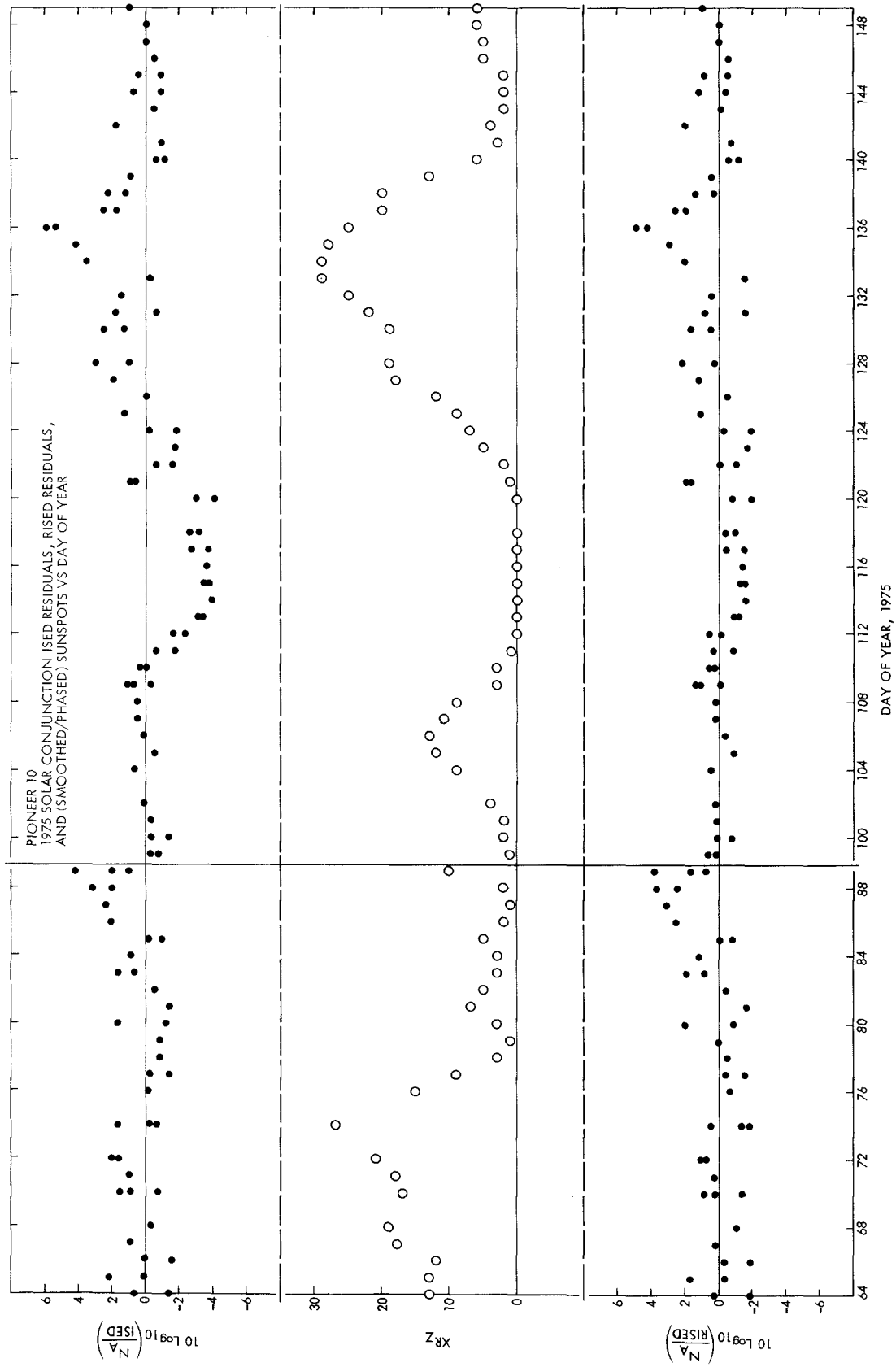

Fig. C-1. Pioneer 10 1975 solar conjunction ISED residuals, RISED residuals, and smoothed-phased sunspots versus day of year

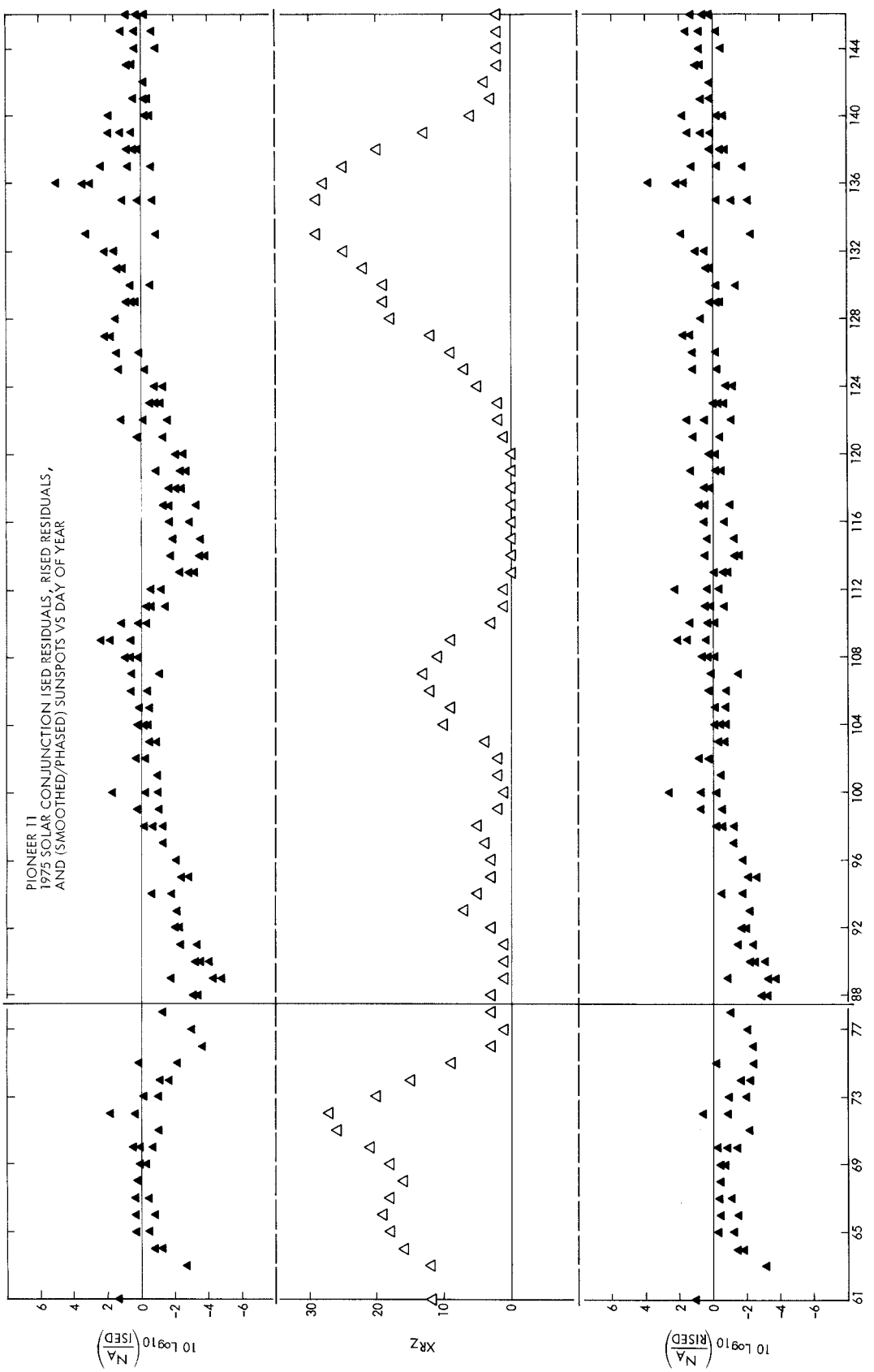

Fig. C-2. Pioneer 11 1975 solar conjunction ISED residuals, RISED residuals, and smoothed-phased sunspots versus day of year

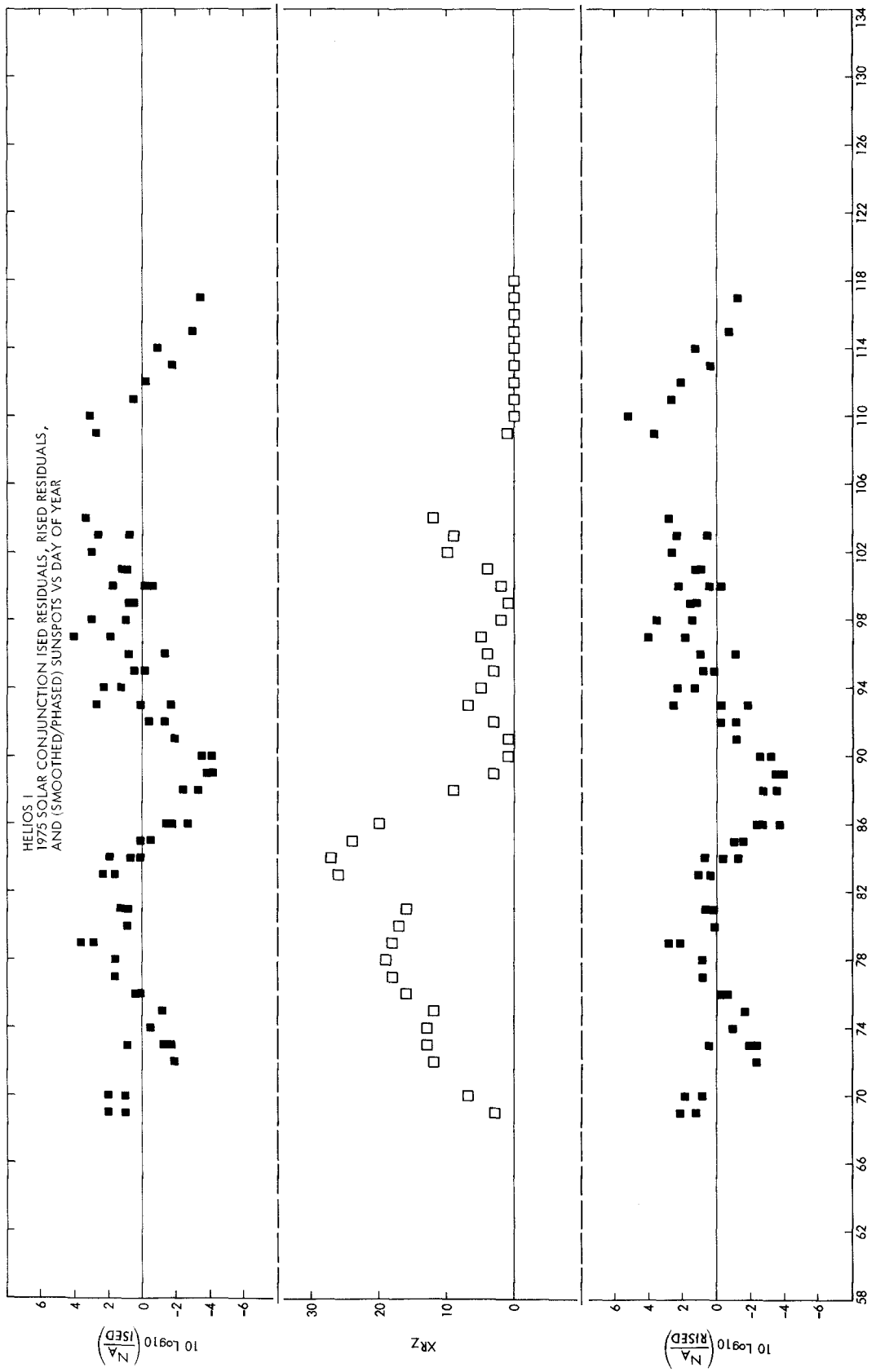

Fig. C-3. Helios 1 1975 solar conjunction ISED residuals, RISED residuals, and smoothed-phased sunspots versus day of year

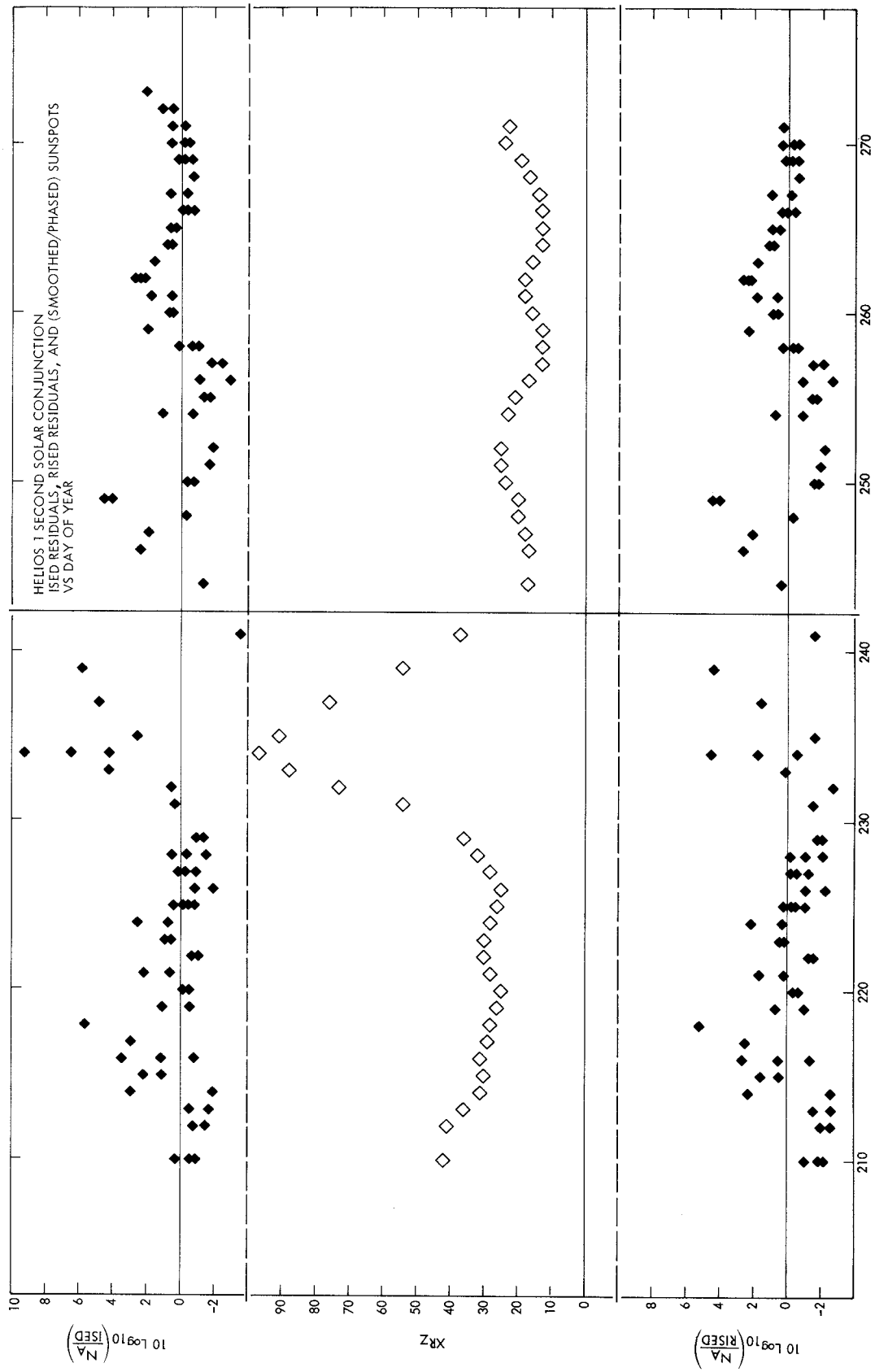

Fig. C-4. Helios 1 second solar conjunction ISED residuals, RISED residuals, and smoothed-phased sunspots versus day of year

Appendix D

Observed Noise and the RISED Model versus Day of Year

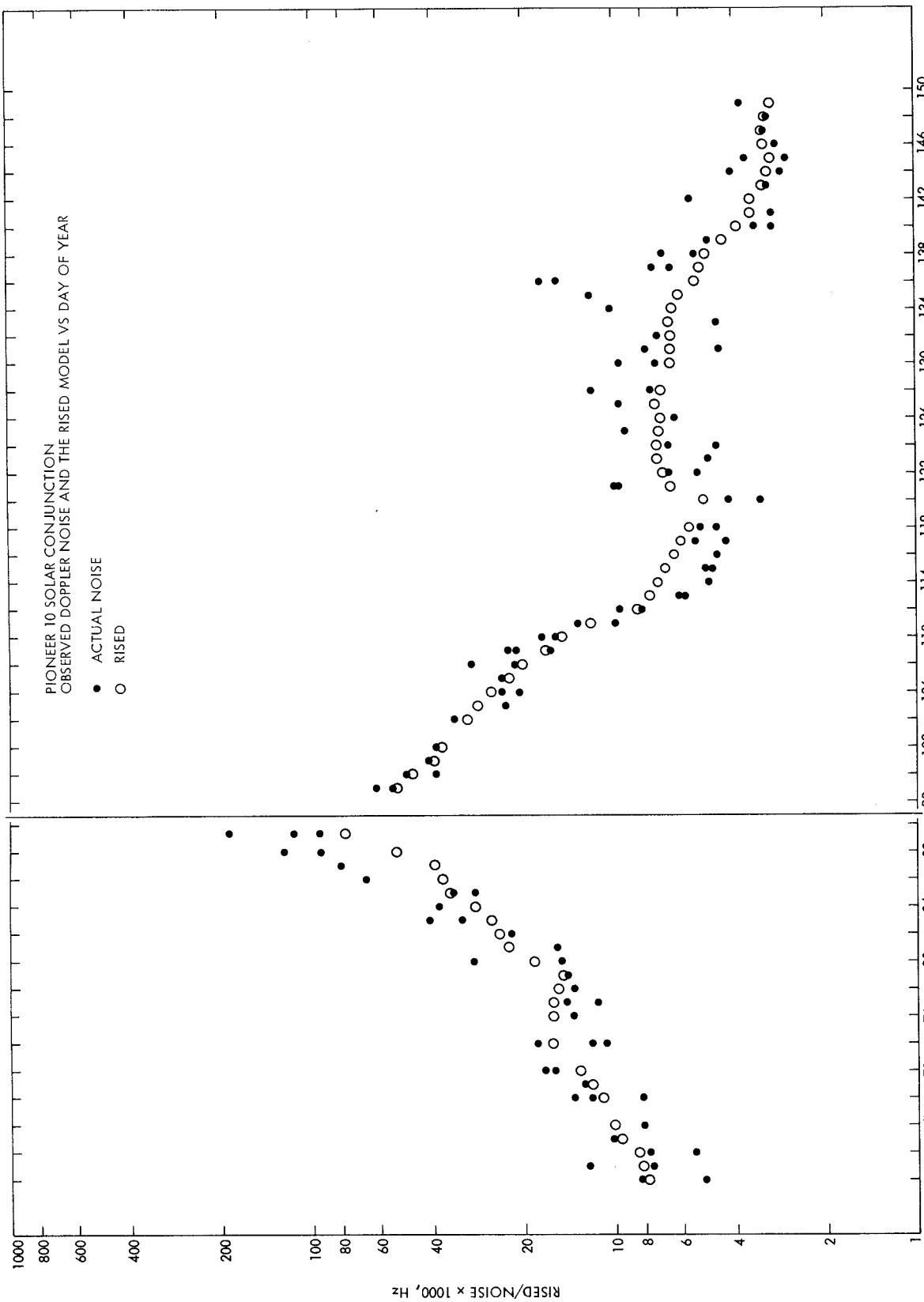

Fig. D-1. Pioneer 10 solar conjunction observed doppler noise and the RISED model versus day of year

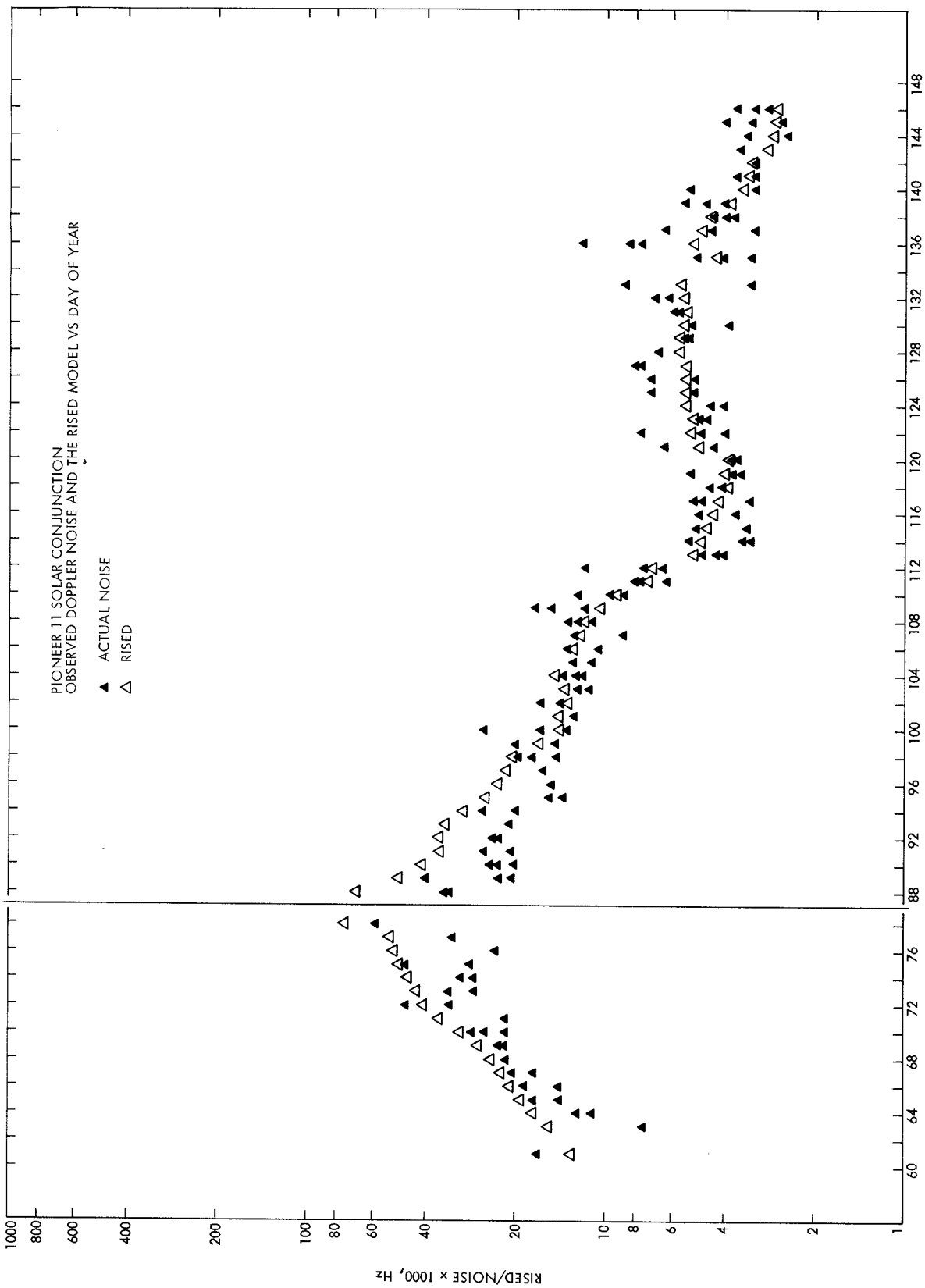

Fig. D-2. Pioneer 11 solar conjunction observed doppler noise and the RISED model versus day of year

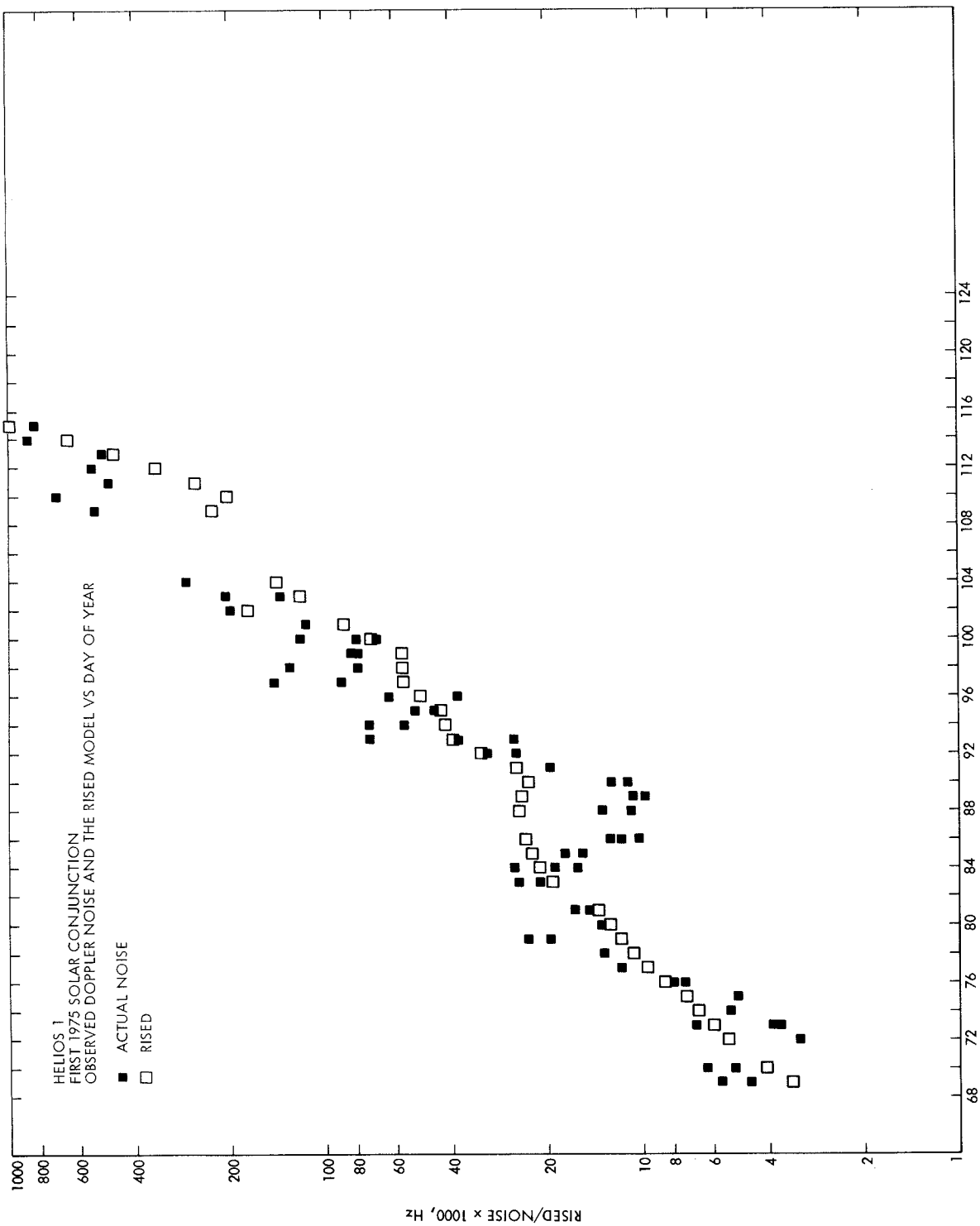

Fig. D-3. Helios 1 first 1975 solar conjunction observed doppler noise and the RISED model versus day of year

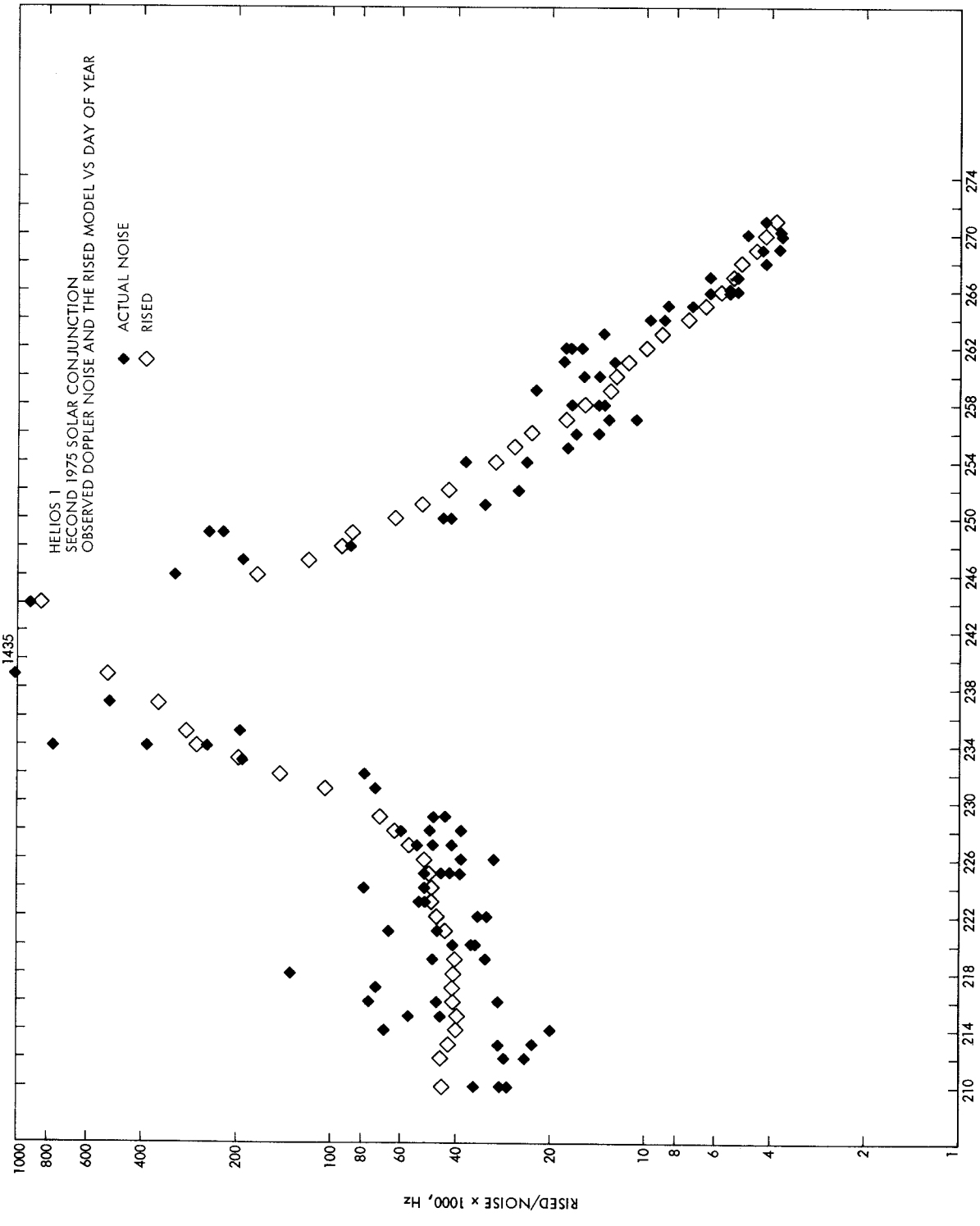

Fig. D-4. Helios 1 second 1975 solar conjunction observed doppler noise and the RISED model versus day of year

Appendix E

Observed Noise versus the RISED Model

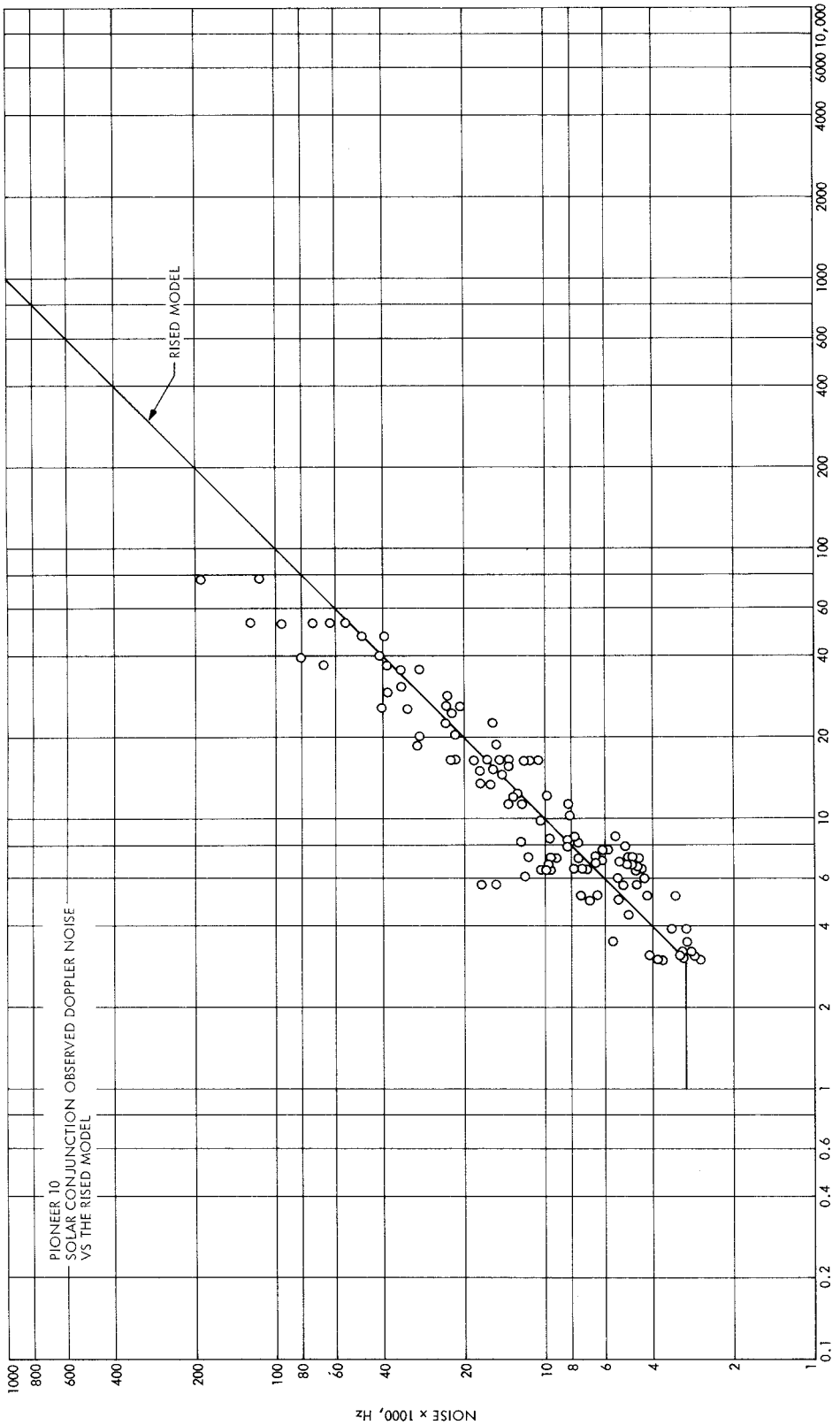

Fig. E-1. Pioneer 10 solar conjunction observed doppler noise versus the RISED model

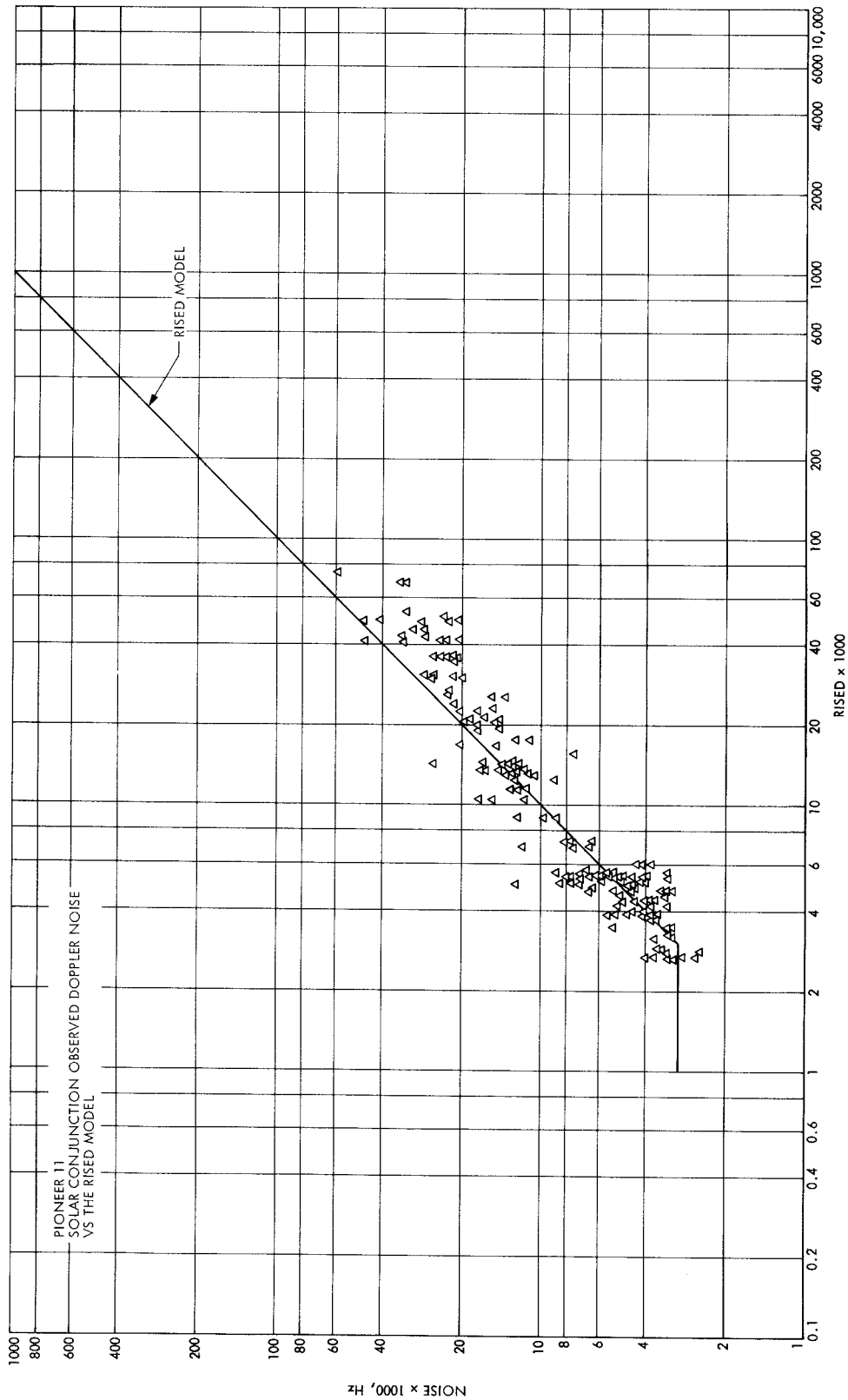

Fig. E-2. Pioneer 11 solar conjunction observed doppler noise versus the RISED model

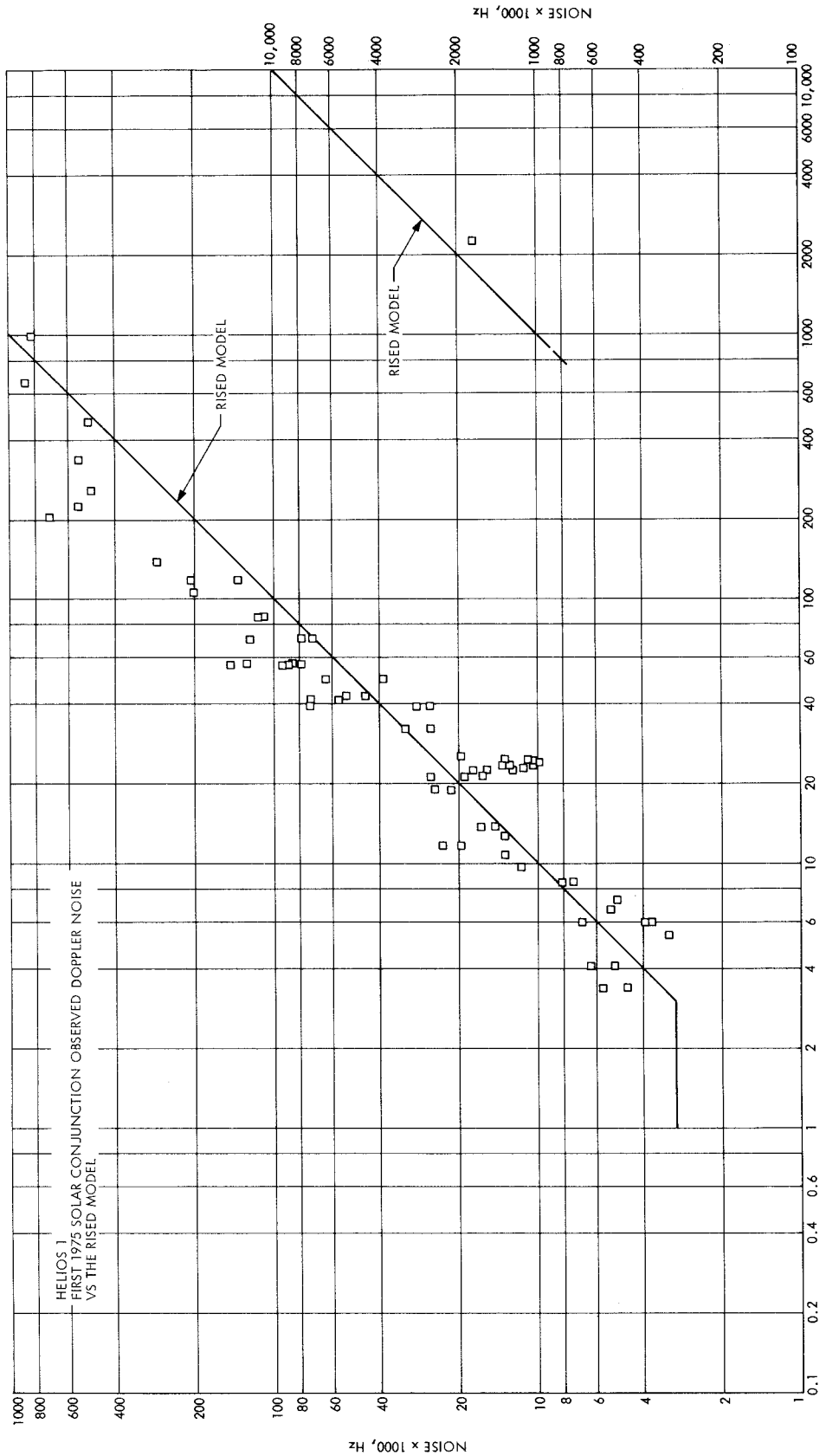

Fig. E-3. Helios 1 first 1975 solar conjunction observed doppler noise versus the RISED model

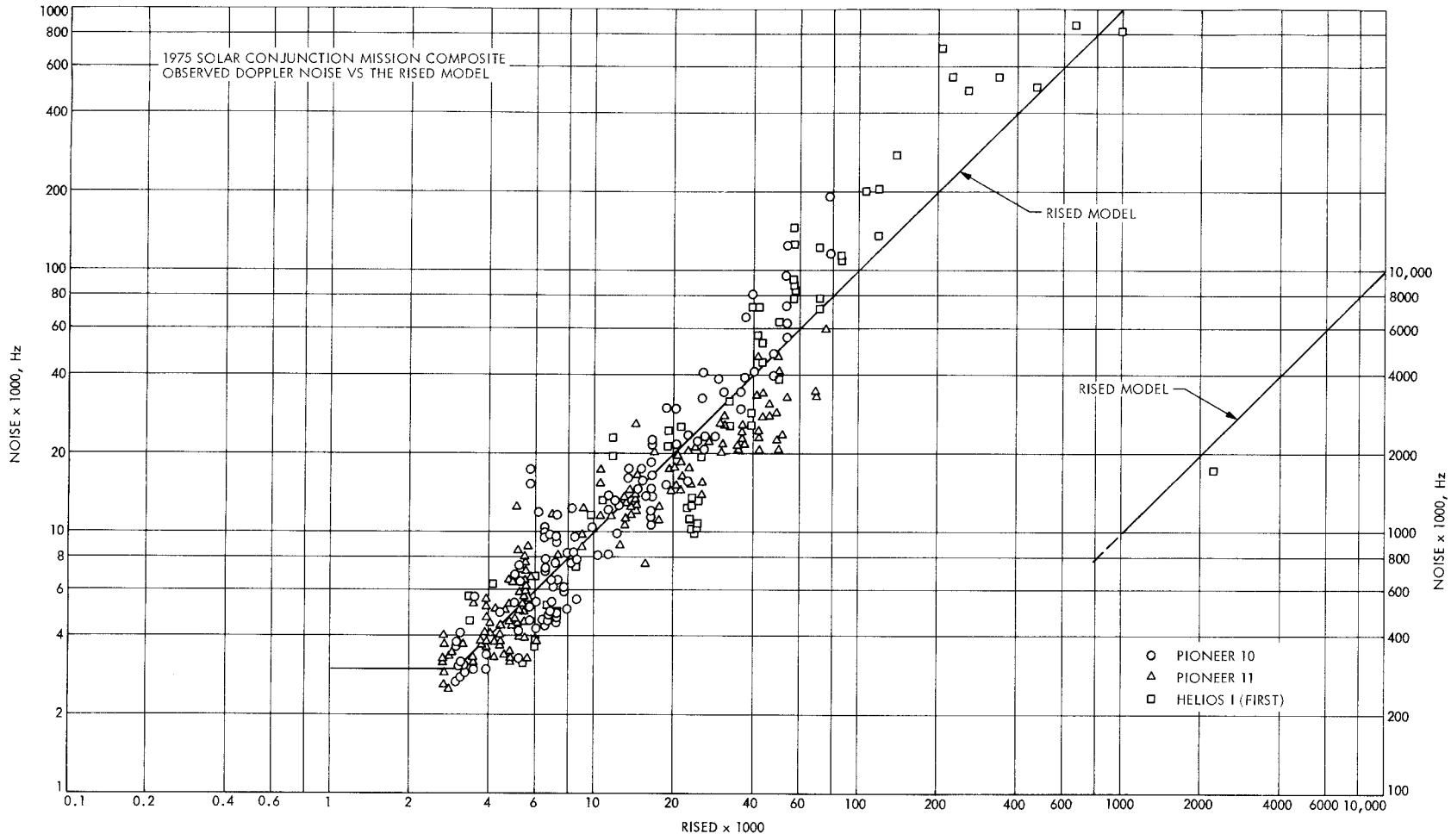

Fig. E-4. 1975 solar conjunction mission composite observed doppler noise versus the RISED model